Theses and Dissertations   1. Thesis and Dissertation Collection, all items

1994-12

Spectral mixing of camouflaged targets

Chandler, John Wells.; Lyon, Suzanne Elizabeth

Monterey, California. Naval Postgraduate School

http://hdl.handle.net/10945/42789

NAVAL POSTGRADUATE SCHOOL
MONTEREY, CALIFORNIA

THESIS

SPECTRAL MIXING OF CAMOUFLAGED TARGETS

by

John Wells Chandler
and
Suzanne Elizabeth Lyon

December, 1994

Thesis Advisor: Richard C. Olsen

Approved for public release; distribution is unlimited.

REPORT DOCUMENTATION PAGE

1. AGENCY USE ONLY *(Leave blank)*	2. REPORT DATE December, 1994	3. REPORT TYPE AND DATES COVERED Master's Thesis

4. TITLE AND SUBTITLE SPECTRAL MIXING OF CAMOUFLAGED TARGETS	5. FUNDING NUMBERS
6. AUTHOR(S) Chandler, John W. and Lyon, Suzanne E.	

7. PERFORMING ORGANIZATION NAME(S) AND ADDRESS(ES) Naval Postgraduate School Monterey CA 93943	8. PERFORMING ORGANIZATION

9. SPONSORING/MONITORING AGENCY NAME(S) AND ADDRESS(ES)	10. SPONSORING/MONITORING

11. SUPPLEMENTARY NOTES The views expressed in this thesis are those of the author and do not reflect the official policy or position of the Department of Defense or the U.S. Government.

12a. DISTRIBUTION/AVAILABILITY STATEMENT Approved for public release; distribution is unlimited.	12b. DISTRIBUTION CODE

13. ABSTRACT *(maximum 200 words)*

A fundamental problem in target detection is the separation of a target and its background, particularly when the target is camouflaged. It is possible to discern camouflaged objects in vegetative backgrounds using reflected light in the visible and infrared range. Reflectance data was taken of five camouflage nets draped over various vehicles with a predominately green background. The aim of this analysis was to reconstruct the spectrum of the observed scene using a linear combination of individual basis spectra called "pure" endmembers. Linear spectral mixing assumes that the observed spectral radiance may be modeled as a linear combination of members of a "pure" endmember spectral mixing library.

The computer algorithm written for this analysis demonstrated the ability to use linear spectral mixing to reconstruct an observed spectrum. The analysis of the abundance mixtures showed that consistent exploitable patterns exist with this type of data. The task of reconstructing the observed spectra was performed with a crude, "non-pure" endmember library. Even greater success could be achieved with a more sophisticated and complete library.

14. SUBJECT TERMS spectral reflectance, plant spectrums, camouflage, linear spectral mixing			15. NUMBER OF PAGES 95
			16. PRICE CODE

17. SECURITY CLASSIFICATION OF REPORT Unclassified	18. SECURITY CLASSIFICATION OF THIS PAGE Unclassified	19. SECURITY CLASSIFICATION OF ABSTRACT Unclassified	20. LIMITATION OF ABSTRACT UL

SPECTRAL MIXING OF CAMOUFLAGED TARGETS

John W. Chandler
Lieutenant , United States Navy
B.S., United States Naval Academy, 1987

and

Suzanne E. Lyon
Lieutenant, United States Navy
B.S., United States Naval Academy, 1987

Submitted in partial fulfillment
of the requirements for the degree of

MASTER OF SCIENCE IN APPLIED PHYSICS

from the

NAVAL POSTGRADUATE SCHOOL
December 1994

Authors: _____
John W. Chandler

_____
Suzanne E. Lyon

Approved by: _____
Richard C. Olsen, Thesis Advisor

_____
Donald L. Walters, Second Reader

_____
William B. Colson, Chairman, Department of Physics

Accession For
NTIS GRA&I ☑
DTIC TAB ☐
Unannounced ☐
Justification ☐

By
Distribution/
Availability Codes
Avail and/or
Dist Special

A-1

iii

ABSTRACT

A fundamental problem in target detection is the separation of a target and its background, particularly when the target is camouflaged. It is possible to discern camouflaged objects in vegetative backgrounds using reflected light in the visible and infrared range. Reflectance data was taken of five camouflage nets draped over various vehicles with a predominately green background. The aim of this analysis was to reconstruct the spectrum of the observed scene using a linear combination of individual basis spectra called "pure" endmembers. Linear spectral mixing assumes that the observed spectral radiance may be modeled as a linear combination of members of a "pure" endmember spectral mixing library.

The computer algorithm written for this analysis demonstrated the ability to use linear spectral mixing to reconstruct an observed spectrum. The analysis of the abundance mixtures showed that consistent exploitable patterns exist with this type of data. The task of reconstructing the observed spectra was performed with a crude, non-pure endmember library. Even greater success could be achieved with a more sophisticated and complete library.

TABLE OF CONTENTS

I. INTRODUCTION

A fundamental problem in target detection is the separation of a target and its background, particularly when the target is camouflaged. It is possible to discern camouflaged objects in vegetative backgrounds using reflected light in the visible and infrared range. The basis for this ability is that most artificial materials do not reflect infrared light rays to the same extent as living green vegetation. Leverage on this problem is an already established wide knowledge base of plant spectra. The spectral knowledge base of green plants includes how the spectra are altered under various natural conditions and phases of a plant's life.

During World War II, attempts were being made to use chlorophyll paint to mimic the reflected spectrum of green plants. These early efforts were effective only in the visible and not in the infrared. Modern camouflage uses camouflage paints and dyes that have been treated so that they have a high infrared reflectance similar to foliage.

It is the hypothesis of this thesis that knowledge of how individual materials spectra mix together to form the spectrum of a scene can be used to expose camouflaged targets. Specifically how vegetation, camouflage, and a vehicle mix together to form a combined spectrum will be looked at to determine if there is a basis for the development of an algorithm that can be used in the field to simply reverse the process and expose the target.

A series of field experiments were conducted at the Malabar Test Range in Florida in June 1994. Spectra were taken using five ultra-light-weight camouflage nets. These nets are various defense contractor companies' attempts to meet the specifications for the Army's Ultra-Light-Weight Camouflage Net System (ULCANS), and are not type classified. They are not in the U.S. government inventory system at the time of this writing. Spectra were taken of several targets with and without the camouflage. The analysis done below is designed to determine if the targets or camouflage nets can be uniquely identified.

II. BACKGROUND AND THEORY

The target identification problem requires a clear understanding of the nature of visible and infrared reflections from vegetation. Many of the techniques that are available have been actively used in agriculture for years to detect changes in crops. By using remote sensing spectral data of crops, the estimation of crop acreage, recognition of crop stress, determination of ground moisture, and timely and accurate prediction of crop yield are possible. Airborne sensors are able to receive an integrated view of all these effects, and each crop or vegetation type tends to have a characteristic signature which permits its discrimination. One example is when disease and physiological stresses directly affect the reflectance properties of individual leaves, the most pronounced initial changes often occur in the visible spectral region because of the sensitivity of the chlorophyll to physiological disturbances. Another example of an effect that is visible to the remote sensor is a reduction in total leaf area of the crop due to some sort of stress. Any insect or pest that supplies sufficient plant stress to distort the reflectance signal significantly is a candidate for detection by means of remote sensing.

This section and following sections will familiarize the reader with the evolution of work in this field, the reflective spectrum of vegetation, as well as how various natural conditions affect these spectra.

A. EARLY WORK

Stokes (1862) laid the foundation for the classical theories for calculation of reflected light. He made calculations from Snell's law and Fresnel's formulas for transparent materials, using appropriate coefficients for refraction and absorption to calculate the reflection of light from a pile of stacked plates. Willstätten and Stoll (1918) explained leaf light reflectance and transmittance on the basis of critical reflection of visible light at the cell wall-air interface of spongy mesophyll tissue. Kubelka and Munk

3

(1931) were two German physicists who developed a mathematical description of the attenuation of light in a diffusing medium. Their work, often called K and M theory, was based on the differential equations derived by Schuster (1905). It is interesting that Stokes' equations can be obtained from the K and M representation applied to the special case of stacked plates (Lillesaeter, 1982). Gates *et al.* (1965) described the wavelength dependence of leaf transmittance. Aboukhaled (1966) studied leaf optical properties related to their energy balance and water-use efficiency.

In 1968, Allen and Richardson used the K and M theory to describe near infrared reflectance and transmittance of leaves as measured when the leaves were stacked in a spectrophotometer. Allen applied the theory to a plant canopy of a given depth and random leaf orientation and showed that the spectral reflectance and transmittance of a plant canopy are functions of total leaf area, an absorption coefficient, a scattering coefficient, and a background reflectivity. Allen, Guasman, and Richardson (1970) also applied Stokes' plate theory to leaves stacked in a spectrophotometer. This led to the development of an additional leaf parameter, the Equivalent Water Thickness (EWT) which is required in order to explain the optical properties of leaves in the 1.4 to 2.5 micron wavelength range. They also described the reflectance and transmittance of a leaf in terms of the reflectivity and transmissivity of interfaces within the leaf absorption and scattering coefficients, refractive indices, and the number of air-cavity-cell wall interfaces.

It was soon discovered that the reflectance was also dependent upon the incidence angle of the radiation. Breece and Holmes (1971) showed that reflection from agricultural crops varies with the vertical viewing angle because of the non-Lambertain reflective properties of vegetative materials. Suits (1972) derived a model for predicting bi-directional reflectance properties of a canopy based on geometric and spectral properties of identifiable canopy components.

4

B. SPECTRAL REFLECTANCE OF VEGETATION

1. Description of Vegetative Spectra and their Primary Influences

A typical reflective spectrum of a plant leaf is shown in Figure 1. The curve shows percent reflectance of incident energy over a spectral range of .4 to 2.6 μm. It should be emphasized that the spectral signature is not constant for a given feature. It is dependent on the spectral distribution of the incident radiant flux, on geometric relationships between the exiting energy and sensor angle of view, on atmospheric effects, and on the physical properties of the feature.

Only part of the incident energy is reflected from the leaf. The remainder is either absorbed or transmitted. Radiation that is scattered upward is considered reflected and radiation scattered downward is designated as transmitted. Often, when chlorophyll and to a lesser extent, other pigments or water are present in the leaf, much radiation is absorbed before it escapes the leaf. These pigments and water account for spectral regions of relatively low leaf reflectance and high absorptance. The reflected, transmitted, and absorbed components are closely interrelated, and it is necessary to consider all three in order to evaluate the physical and physiological basis for leaf reflectance. Figure 2 is representative of the relationship between these three components.

The spectrum range being described is .4 to 2.5 μm and can be divided up into three parts. The visible portion of the spectrum is from .4 to .75 μm. The next section is the beginning of the near infrared and extends from .75 to 1.35 μm. The final section is a region in the near infrared that is characterized by high water absorption. It extends from 1.35 to 2.5 μm.

The visible region (.4 to .75 μm) is characterized by absorption by pigments consisting mainly of chlorophylls a and b, carotenes, and xanthophylls. Chlorophylls a and b are the most frequently found forms of chlorophyll but altogether about ten

5

different forms have been identified, each with a unique absorption spectra. The energy absorbed selectively at certain wavelengths by chlorophyll will be converted into heat or fluorescence, and converted photochemically into stored energy in the form of organic compounds through photosynthesis. The main pigments absorb in the same region, in the vicinity of .445 μm in the blue, but only chlorophyll absorbs in the red in the vicinity of .645 μm (Gates, 1965). The Manual of Remote Sensing lists absorption of light by chlorophyll in the blue (.45 μm) or red (.68 μm) at 70-90 percent.

Gates *et al.* (1965) provides an excellent discussion of the processes of reflection in the near infrared from .75 to 1.35 μm. Plants absorb very efficiently throughout the visible regions of the spectrum where energy is required for photosynthesis. Immediately to the long wavelength side of the red chlorophyll absorption band the reflectance and transmittance of plant leaves increase dramatically, resulting in the absorptance falling to a very low level. The main influence on reflectance in this region is the internal cellular structure of the leaf. Knipling (1970) warned that the infrared reflectance in this region had sometimes erroneously been attributed to the chlorophylls. Actually, the absorption spectra of isolated chlorophylls indicate that the pigments are completely transparent to infrared radiation. Little or none of the infrared radiation is absorbed internally. Generally, 40 to 60 percent is scattered upward through the surface of incidence (reflected), and the remainder is scattered downward (transmitted). Woolley (1971) confirmed that the pigments do not absorb in this region by extracting the pigments from the plants and testing the pigment reflectivity by itself. This drop in absorption occurs precisely throughout the frequency range where direct sunlight incident on plants has the bulk of the energy. If plants absorbed this energy as efficiently as they do in the visible, they would become too warm and their proteins would be irreversibly denatured. This frequency range is a region of high reflectance and low absorption.

The final region, 1.35 to 2.5 μm, is influenced somewhat by internal structure but is more prevalently affected by water concentration in the leaf tissue. Strong water bands occur at 1.45 and 1.95 μm. The quantity of liquid water present in leaf biomass was

related to a term called the Equivalent Water Thickness (EWT) by Allen (1969). EWT indicates the thickness of a sheet of water that can completely account for the absorption spectrum of a leaf in this spectral range. Figure 3 superimposes the regions of high water absorption on the spectrum of a green leaf.

This section can be summarized by stating that plants absorb efficiently where they require the energy, absorb poorly in the near infrared to keep from becoming overheated, and absorb in the far infrared in order to be efficient radiators.

2. Leaf Structure

The internal organization of the leaf is well adapted for its major function of photosynthesis, gas exchange, and transpiration. A good description of leaf morphology is given by Gates *et al.* (1965) and by Dengler (1982). Figure 4 is a drawing of a typical leaf structure. The top layer of cells is the upper epidermis. The epidermis is usually made up of flat tabular cells which may be elongated. Regardless of shape, epidermal cells always fit tightly together without intercellular spaces, and they secrete a layer of hydrophobic substances, such as cutin and waxes on the outside surface. Both of these adaptations reduce water loss. The layer of cutin is referred to as the cuticle.

The epidermal cells usually contain colorless plastids rather than chloroplasts. Thus, the epidermis is a clear unpigmented layer of cells which allows light to penetrate to the subjacent photosynthetic tissue and reflects very little. The long narrow cells below the upper epidermis are palisade cells. The cells below the palisade cells are spongy-mesophyll cells. These are loosely packed parenchyma cells separated by intercellular spaces. Within these cells are numerous green chlorphyll-containing chloroplasts. It is here that oxygen and carbon dioxide exchange takes place for photosynthesis and respiration. The lower epidermis is like the upper epidermis, except a stoma or port is present where gases enter and leave a leaf.

7

The cellular structure of the leaf is large compared to the wavelengths of light. Typical cell dimensions will be 15 by 15 by 60 μm for palisade cells and 18 by 15 by 20 μm for spongy parenchyma cells. The epidermal cells are of the same order of dimension as the spongy parenchyma cells. The cuticular layer is highly variable in thickness but often is only 3 to 5 μm thick which in terms of magnitude is comparable to infrared wavelengths. The chloroplasts suspended within the cellular protoplasm are generally 5 to 8 μm in diameter and 1 μm in width. As many as 50 chloroplasts may be present in each parenchyma cell. Within the chloroplast are long slender strands called grana within which the chlorophyll is located. The grana may be .5 μm in length and .05 μm in diameter. Clearly, the grana are of the dimension of the wavelength of light and may produce a considerable scattering of light entering the chloroplast. The chloroplasts are generally more abundant towards the upper side of the leaf in the palisade cells and hence account for the darker appearance of the upper leaf surface. (Gates *et al.,* 1965)

Leaf anatomies typically have a great deal of open structure in the form of intercellular spaces, which contain moisture-saturated air. The materials of the leaf which are important from the standpoint of light and radiation are: cellulose of the cell walls, water containing solutes (ions, small and large molecules such as protein and nucleic acid) within the cells, and intercellular air spaces and pigments within the chloroplasts. The pigments generally found in chloroplasts are chlorophyll (65%), carotenes (6%), and xanthophylls (29%), although the percentage distribution can be highly variable.

Willstätten and Stoll (1918) were the first workers to recognize the internal reflection mechanism of leaves, but they, and many other workers since, perhaps overemphasized the role of the spongy mesophyll and its large air cavities in relation to that of other interior parts of the leaf. Mathematical analyses of theoretical models and photomicrographs of cross sections of leaves suggest that the important parameter in determining the level of reflectance is the number or total area of air-wall interfaces and not the volume of air space. In this regard, the palisade mesophyll of a leaf probably is as important as the spongy mesophyll in the internal scattering of radiation. Many small air

cavities exist between adjacent palisade cells, and the area of exposed cell walls in this region probably is as large and perhaps even larger in some cases as in the spongy mesophyll which generally has larger air cavities and fewer cells. (Knipling, 1970)

3. Vegetative Canopies Versus Leaf Spectra

Knipling (1970) investigated the differences between the reflective spectrum of a single leaf and that of a vegetation canopy. Figure 5 shows the geometry of the canopy problem. The reflectance properties of single leaves are, of course, basic to understanding the reflectivity of an entire plant or vegetation canopy in a field situation, but the single leaf data cannot be applied directly without modifications. There are both quantitative and qualitative differences in the two types of spectra. On a percentage basis the reflectance from a canopy is considerably less than that from a single leaf because of a general attenuation of radiation by variations in illumination angle, leaf orientation, shadows, and nonfoliage background surfaces such as soil.

The visible and near infrared reflectance from a nearly continuous broad-leaved canopy typically might be about 5 percent and 35 percent respectively, whereas the corresponding values for a single leaf are about 10 and 50 percent (Steiner and Gutermann, 1966). In this case the levels of visible and infrared reflectance from the canopy are about 40 and 70 percent, respectively, of the levels from a single leaf. The relatively smaller reduction in infrared reflectance is due to a compensating factor. Much of the incident infrared energy transmitted through the uppermost leaves is reflected from lower leaves and retransmitted up through the upper leaves to enhance their reflectance. (Myers *et al.*, 1966).

C. INFLUENCES ON REFLECTIVE SPECTRA OF VEGETATION

1. Effects of Water Content

Different biophysical properties of vegetated surfaces control the interaction of the leaf with the incident solar irradiance. In the .75 to 1.35 μm near infrared region, the spectral properties of a leaf are associated with its morphology and, to a lesser extent, its water content Gausman *et al.* (1969). Following the loss of water from the intercellular spaces, further dehydration of the leaves results in changes in the internal structure Thomas *et al.* (1971). The infrared reflectance of a dried leaf is largely that of a diffuse cellulose reflectance, while the fresh leaf infrared reflectance curve depends on a combination of diffuse reflectance with water absorption bands Woolley (1971). As indicated previously by Allen's research (1969, 1970), the quantity of liquid water present in the leaf biomass of the plant canopy largely controls the resulting 1.3 to 2.5 μm spectral reflectance. This region is sensitive directly to leaf water content. Allen showed that the absorption spectra was not statistically different from that of the liquid water contained in the leaf's EWT. Generally speaking, at wavelengths where water absorption is high, leaf absorption is low, (see Figure 3).

Figure 6 shows the effect of dehydration on leaves. It is evident that dehydration greatly increases reflectance over the entire .5 to 2.5 μm wavelength interval. Thomas *et al.* (1966) found that reflectance increased as relative turgidity decreased below values of 80 percent. Relative turgidity is used to measure water stress in plants. It is the actual leaf water-content expressed as a percentage of the saturation water content. Water stress refers to the combination of abiotic conditions which produce serious internal plant water deficits which limit photosynthesis and restrict plant growth. The limitation of soil water availability to plants is a common environmental occurrence. The increase in reflectance in the visible region of the spectrum (.4 to .75 μm) does not always happen since drying may decrease reflectance in this region. Often, however, the influence of water is masked

by leaf pigment content. Leaves of plants under water stress generally appear darker green than leaves of plants not stressed, thus they reflect and transmit light differently. (Thomas *et al.,* 1971)

Johannsen (1969) found that leaf moisture and pigment changes are closely related and are hard to separate. His results showed that the water absorption bands (1.45 μm and 1.95 μm) are inversely related to leaf moisture. The green color response and chlorophyll absorption (.53 μm and .64 μm respectively) also showed a high negative correlation with leaf moisture. The pigments in the leaf were affected by changes in leaf moisture in a very short time. Tucker (1980) found that the spectral regions of greatest change in leaf reflectance as a function of equivalent water thickness were the 2.1 to 2.35 μm range followed by the 1.83 to 1.88 μm range and, lastly, the 1.42 to 1.82 μm and 1.9 to 2.05 μm ranges.

2. Effects of Plant Age

It is probable that the near-infrared reflectance is a function of the cell shape and size as well as the amount of intercellular space. Initially, the mesophyll of the very young leaf consists primarily of spongy parenchyma with considerable air spaces which are favorable to the mechanism of internal reflection. Then, as the leaf matures, the cells enlarge, crowd together, and reduce the intercellular space thus reducing the reflectance. It would then appear that during leaf senescence, the deterioration in plant leaves, flowers, fruits, stems, and roots, as they near the end of their functional life, causes the cell structure and intercellular space relationship to become favorable for increased reflectance. Gates (1965) Figure 7 shows the increased reflectance with maturity associated with leaf senescence.

Most herbaceous annual plants have a progressive senescence from the younger to older leaves. During leaf senescence, starch, chlorophyll, protein and nucleic acid components are degraded. Light reflectance usually increases markedly in the .55 μm

11

band when chlorophyll degradation takes place. Leaf senescence leads to decreased infrared reflectance and the infrared plateau at about .75 μm is usually reduced considerably. (Myers, 1983)

The term "collapse of the mesophyll" has often been used to predict and explain decreases in infrared reflectance. It was presumed that, when leaves wilted and shriveled during senescence and dehydration, many of the reflective interfaces were eliminated as internal air space was reduced and cell walls came together. Even though the internal leaf volume decreases, microcavities remain between the walls and the number of interfaces may actually increase as adjacent cells split apart and as living cell contents shrink away from interior cell walls. Also, the reorientation of the cell walls (Sinclair, 1968) and the receding of water from the wall surfaces into the microfibrillar network may increase their radiation-diffusing capacity and thus account for increases in leaf reflectance. The infrared reflectance eventually decreases in advanced stages of leaf senescence (Knipling, 1969), but this more than likely is caused by an actual breakdown or deterioration of cell walls rather than by a collapse or reduction in the spongy mesophyll air volume. (Knipling, 1970)

3. Effects of Leaf Damage

Remote sensing detects leaf damage indirectly, as leaf damage will ultimately affect the normal functioning of the plant. One of the first visual symptoms of physiological damage is yellowing of the foliage, but this may not be the first change in spectral reflectance. The first changes in the spectral reflectance pattern, which in many circumstances is an increase in reflectance, occur in the near infrared region. Thomas *et al.* (1966) and Gausman (1977) stated that both crystals and cytoplasm as well as other structures contributed to the reflectance of near infrared light. If physiological damage affects the functioning of the cell, then it is quite probable that it also affects the size and number of cellular crystals and the amount of cytoplasm. Continuing chronic damage

eventually causes a deterioration of chloroplasts. This change in physiology is generally visually noted as a yellowing of the foliage. The final generalized change is the reddening of the dead foliage. This change is accompanied by a continuing shift of the visual peak towards red, and thus an increase in red reflectance is noted. At this point, the near-infrared reflectance may be affected by environmental factors. If the foliage is air-dry, the dried cells are highly reflective of near infrared and, if the dead foliage is wet, the reflectance is decreased, since water is a well-known poor reflector of near infrared.

4. Effects of Angle of Incidence and Background Contributions

Reflection from agricultural crops varies with the vertical viewing angle because of the non-Lambertain reflective properties of vegetative materials. The results for different viewing angles indicate that the canopy geometry may occur in non-Lambertain character. The lower canopy layers have less influence on the reflectance unless the upper layers are poorly populated. (Breece and Holmes, 1971) Rao *et al.* (1979) investigated the bidirectional reflectance of crops and the soil contribution. He found that the Leaf Area Index (LAI) and the percentage of ground cover are significant factors that influence the directional effects of spectral reflectances.

The reflectance (ρ) of any area (A) which is partially covered with vegetation may be expressed approximately as a composite reflectance given by:

$$\rho = (A_v \rho_v + A_s \rho_s)/A \qquad (2\text{-}1)$$

where A_v =vegetation area and A_s=soil area (Janza, 1975). The radiance value, seen by any remote sensor, of a vegetated area is a mixture of radiance values of the plant canopy and of the soil background. Plants in their early growth stages cover only a fraction of the soil background.

13

Condit (1970) examined 160 soil samples from across the United States. He classified them all into three general types with respect to their curve shape in the .32 to 1 μm range. The three general shapes of the spectra of these soil types are shown in Figure 8. Soil has a higher reflectance in the visible spectrum, and the surface of mixed soil and vegetation reflects less than bare soil. The reverse is true for the infrared, as plants have a higher reflectance than the soil. The relative variation of reflectance for sod is much greater in the infrared part of the spectrum than in the visible part. Soil reflectance also varies with soil type, water content, and tillage. Condit's type 1 soil has the distinguishing feature that, over any range of wavelengths, the slope, with minor exceptions, either increases or is nearly constant. In type 2, the reflectance increases fairly rapidly from .32 to .45 μm, where a slight or even moderate dip in the slope occurs, followed by an increase in the slope at about .48 μm. At about .58 μm, another decrease in the slope occurs. From .6 μm to about .7 μm, a slight to moderate dip in the slope is generally present. At about .75 μm, the slope decreases again and beyond that the slope usually changes very little with increasing wavelength. In type 3, the slope of the curve increases at a moderate rate from the ultraviolet region to about .53 μm, then rises sharply to about .58 μm, where a definite decrease in the slope occurs. From about .62 to .74 μm, a slight to moderate dip in the slope is usually present. At .74 μm, another definite decrease in the slope occurs, often dropping to or near zero.

Lilllesaeter (1982) also studied the effects of a background on reflectance and his work is discussed in the following section: Mathematics and Modeling.

5. Effects of Atmospheric Attenuation

Remote sensing of plant canopy water status from ground, aircraft, or orbital altitudes requires knowledge of atmospheric transmission characteristics and solar intensity. Atmospheric transmission/absorption and the intensity of the incident spectral irradiance are closely linked in reflective remote sensing. Not only must sufficient

incident spectral irradiance be present at the earth's surface to achieve a required signal-to-noise ratio for the sensor in question, but atmospheric conditions must be such as to allow largely unattenuated transmission of resulting target spectral radiance to the aircraft or satellite sensor platform altitude. Atmospheric absorption in certain wavelength regions precludes utilization of many areas of the .4 to 2.5 μm spectral region and the low energy output of the sun beyond 2.5 μm greatly restricts reflective use of this area. Remote sensing in the .4 to 2.5 μm region is thus greatly restricted by atmospheric and irradiational conditions. (Tucker, 1980)

D. MATHEMATICS AND MODELING

Lillesaeter (1982) presented a simple approach to modeling a partly transmitting plant that is influenced by a background. With irradiance (I) impinging upon unit area of the leaf, the reflected radiation (R1) can be considered to be made up of two components (see Figure 9): the inherent leaf component (R), i.e., the radiation reflected from the leaf with an ideally black background; and the background component (R'), i.e., the radiation reflected from the non-black background, modified by the transmittance (τ) of the overlying leaf.

Thus, the reflected radiation can be expressed as

$$R1 = R + R' = rI + r'\tau^2 I, \tag{2-2}$$

where r and r' are the reflectances of leaf and background respectively. The apparent reflectance of a single leaf is

$$r_1 = \frac{R1}{I} = r + r'\tau^2, \tag{2-3}$$

15

r being the leaf component and $r'\tau^2$ the background component. Generally, the quantities r, r', and τ vary with the wavelength. In the above equation, r' can be regarded as a known instrumental parameter, whereas r and τ are sample variables. Taking spectral measurements of the leaf placed initially on a dark (D) background, and subsequently on a light (L) background, one obtains the following relationships

$$r_{1D} = r + r'_D \tau^2 \qquad (2\text{-}4)$$

$$r_{1L} = r + r'_L \tau^2. \qquad (2\text{-}5)$$

Eliminating r and solving for τ^2, the two-way transmittance of the leaf can be determined.

$$\tau^2 = \frac{r_{1L} - r_{1D}}{r'_L - r'_D}. \qquad (2\text{-}6)$$

With appropriate values established for background reflectance and leaf transmittance, the inherent leaf reflectance r can be derived from either Equation 2-4 or 2-5. Identical leaves are then superimposed on one another and for τ less than one, the expression for inherent leaf reflectance becomes:

$$\lim_{N \to \infty} r_N \equiv r_\infty = \frac{\tau}{1 - \tau^2}. \qquad (2\text{-}7)$$

Lillesaeter reached the following conclusions modeling with Equation 2-7: (1) In opaque cases ($\tau \sim 0.05$), as in the visual part of the spectrum, one leaf suffices: reflectance measurements are not influenced by the background. (2) With intermediate opacities, as in parts of the near infrared, a few leaves may be required to eliminate the effect of the background. (3) In the transmitting part of the near infrared, up to eight leaves may be required for r_∞ to be reached. (4) Irrespective of transmittance, the inherent reflectance of a single leaf can be measured directly, provided that the background reflectance is less than about 0.03. Lillesaeter's results were consistant with Guasman's *et al.* (1973) and

16

Allen's (1968) work. They found that reflectance against a soil background increases as the number of leaf layers in the canopy increase until a stable value of reflectance is attained (R_∞). In the visible, R_∞ is reached when plants reach a leaf area index (LAI) of two. Leaf area index is the cumulative one-sided leaf area per unit ground area measured from the canopy top to a plant at a given distance from the ground. Myers *et al.* (1966) In the near infrared, a LAI of about eight is required because of the transparancy of leaves in this region.

E. CAMOUFLAGE BASICS

1. The Camouflager

The goal of the camouflager is to use the materials at hand to decieve the enemy about intentions, troop strength, location, land use, etc. He must, of course, be able to mimic his suroundings or coverings in the visible region to decieve the immediate onlooker, but the deception must also withstand the skill of a photointerpreter who has many ways to see beyond the camouflage. Using steroscopic photography or measuring shadows he can determine whether the size of the object matches with the apparent object (Reit,1978). Multispectral imagery, such as that available from a LANDSAT sattelite, allows for computer-assisted terrain classification or change detection (DMA, 1994). Because detection techniques become more time intensive and expensive as they become more complex, the camouflager must decide how thourough his deception must be based on what techniques he expects will be used against him.

2. Deception in the Visible Region

Camouflage in this region is designed to fool the human observer or photointerpreter who is using only photography. There are many ways to achieve

deception in this region including paint, nets, artificial foliage, artificial tanks or bomb damage, and even an object's size. These methods are used individually or collectively to convince the observer he is seeing something other than what is actually there. Some examples of the clues an observer uses to identify objects are in Figure 10. (Department of the Army, 1968). Other clues in addition to shadow, relative position and shape are texture, color, and movement.

One of the simplest ways to begin is to camouflage the outlines of the object in question. This can be seen in a soldier's fatigues or on his truck. The distinctive military clothing and paint is actually to help the soldier blend into the surroundings. A tree or bush, for example, is not a solid pattern of green. Light and dark spots appear randomly because of lighting, leaf spacing, and vegetation density. The sharp edges and monotones of conventional clothing or vehicles are therefor easy to spot because they break the natural pattern. The amorphous shapes of the light and dark patches in military camouflage patterns are designed to blend into the surroundings, taking away the obvious straight edges and color contrast. For an example see Figure 11. Painting patterns on the object to be camouflaged can deceive the viewer about use or damage also. If the camouflager wants the viewer to believe a building is bomb damaged, he can create fake damage by painting a bomb crater on the building.

Camouflage nets like the ones used in this analysis serve many purposes for the camouflager. Nets are most often used to help small buildings and aircraft blend into the surrounding terrain and are usually temporary in nature. The net is colored to match the terrain and vegetation. It gives the distinctive shape of an aircraft a more amorphous form when the net is draped over the aircraft. Using a net as a canopy can serve to hide stores or small command posts. (Mendelsohn, 1989)

Another method of deception is to modify the surroundings. One does not normally expect to find a bomb factory in the middle of a farm, for example. During the second world war the Lockheed-Vega aircraft factory in Burbank, California was

18

disguised as a rural community (Reit, 1978). This type of camouflage is for long term deception.

All types of camouflage require constant upkeep to ensure their continued viability. Simple camouflage like paint or nets requires replacement due to normal wear and tear while more complex camouflage like the Lockhead-Vega plant work requires constant vigilance to maintain. Longterm camouflage also requires constant minor modification to give the appearance of use. For example, photo reconnaisance of dummy German airfields during World War II showed the aircraft parked in the same spots and at the same angles every time the photos were taken. If the airfield had actually been in use the planes would have been in random positions each time the reconnaisance aircraft flew over. The British took pains to move their dummy aircraft daily and add other signs of life to their longterm decoys in order to avoid this obvious flaw in the camouflage (Mendelsohn, 1989).

Lighting and shadows can be an important part of camouflage. From directly overhead a building is mostly outline. It has no depth. Shadows from the building give the observer some sense of its vertical extent unless, however, the sun is also directly overhead. An example would be the Washington Monument. From directly overhead, with no shadows, the observer would see a white square. Move the sun from its zenith, and suddenly the monument has depth. The pyramid shaping at the top can be distinguished by the shadows it throws on itself, and the long thin shadow of the monument clearly shows its extensive height (Figure 10, left). It is for this reason that paint alone is not usually enough to effectively camouflage an object. The camouflager must be able to give his deception apparent depth at various angles of lighting and observation.

Another clue an observer might use to identify an object is apparent texture and here again lighting is important. The amount of light reflected by an object in a given direction depends on the object's texture and the angle of incidence of the light. A scout carefully camouflaged with deceptive clothing and artificial foliage may be detected if he

allows the sun to reflect off of his binocular lens. This anomolous reflection makes it clear to the observer that there is a relatively smooth surface where there should be only relatively rough ones. The camouflager should understand this and carefully use textures or mimic them in his deception.

3. Deception in the Infrared Region

Understanding how objects reflect in the infrared regions can make the identification of areas or items of interest much easier. Two objects which reflect similarly in the visible may have completely opposite characteristics in the near infrared or far infrared. For example, a stream winding through a forested region may not be easy to distinguish from the forest in the visible spectrum because they would both reflect mostly in the blue-green region. In the near infrared, however, the stream would stand out clearly because water absorbs and vegetation reflects in that region. Use of this knowledge is limited by the observer's access to infrared imagery and by the atmosphere.

As early as World War II efforts were underway to produce camouflage that also worked in the infrared regions (National Defense Research Committee, 1946). In this way the camouflager could deceive not only the immediate observer, but also the intelligence agent with infrared photography. The nets used in this study are a new attempt to provide camouflage which is effective beyond the visible spectrum.

4. Detection Methods

All detection methods are affected by atmospheric propagation. The various molecules which make up the atmosphere have absorption and transmission bands which are fairly well established. Water and carbon dioxide in the atmosphere have the most impact on transmission of infrared radiation limiting the observer to certain windows. Turbulence in the atmosphere also affects transmission by changing the local index of

20

refraction. This atmospheric turbulence is essentially what causes stars to twinkle. Finally, atmospheric scattering affects transmission over long distances.

The first type of detector is the human eye. It is limited to the visible spectrum and by range; however, a well trained observer can detect very subtle oddities and motion that a picture cannot. An example is a demonstration at the Exploratorium in San Francisco, California. A computer screen has a background and an object with coloring that is identical to the background. The object moves across the screen. The object is visible to the observer because it is moving. Pushing a button stops the movement temporarily and the object disappears into the background.

A human observer also provides real-time information. An observer in the field with a radio can instantly relay information on location and size back to those who need to know. A photograph must be taken, processed, and then sent to the interpreter. All of this takes time.

The next type of detector is the photograph or electronic still imager. The wide variety of cameras, platforms, and films available means that a photograph can provide a wide variety of information without the risk to a human observer. The type of camera determines the field of view and the resolution. The type of film determines what information is available. The platform determines how close one can get to an area of interest and how often pictures can be taken.

A distinct advantage of the photograph over a human observer is that a photograph provides a permanent record for comparison with later observations or with information from other imaging detectors. The angle of view is important when comparing two images. An image or photo taken from an oblique angle will provide different information from one that was taken directly overhead. Two images taken from different angles or sources should be correlated before they are compared (DMA , 1994).

Today's multispectral imaging poses a new challenge to the camouflager. Many of the techniques, that can be used to detect hidden or camouflaged objects, are used in a variety of non-military ways. An example is terrain catergorization. Using multispectral

images from a platform such as a LANDSAT satelitte and some general knowledge of the area in question, comparisons are made pixel by pixel across the bands. The computer plots an average pixel brightness for a given group of pixels. Other pixels which represent similar terrain features should have averages in the same vicinity thus allowing nearby "clusters" to be grouped together as one terrain category (DMA, 1994). Since LANDSAT has seven spectral bands, the camouflager has to design his longterm decoys to reflect appropriately throughout the spectrum.

Short term camouflage does not need to be complex because the platforms from which the observer is able to get data on short notice are not as complex. The advantage of time is also in favor of the camouflager. Short term camouflage is intended only to delay the camouflaged object from being noticed. For example, it may take up to 4 weeks to get data from LANDSAT. If one only wants to hide a missile launcher for an hour, the camouflage does not need to be designed to deceive much beyond the visible.

III. DATA COLLECTION

A. EXPERIMENT SETUP

The data used in this analysis was collected by the Kestrel Corporation using a MultiSpec™ spectrograph by Oriel. The wavelengths and resolution of this instrument depend upon the combination of slit and grating used. The grating used for this data was model number 77411 which has a primary wavelength region of .2 to 1.25 μm with a spectrographic resolution of 0.4 nm. (Oriel data sheet, 1994) The detector used with the MultiSpec™ was the InstaSpec™ II photodiode array detector also manufactured by Oriel. The spectral response of the InstaSpec™ II is .18 to 1.1 μm; however, data collected at the extremes of the detector's usable wavelength range was extremely noisy and was not used in this analysis.

Light incident upon a slit or a diffraction grating is transmitted or reflected in a manner dependent upon the wavelength of the light and the angle of incidence. The instrument used for data collection in this case admits light through a slit. This light is then acted upon by a diffraction grating and exits the spectrometer enroute to the detector (see Figure 12). Both the slit width and the spatial wavelength of the grating may affect the resolution of the instrument.

The diffraction pattern for monochromatic light of wavelength λ through a slit of width D_x and length D_y observed at a distance d is dependent upon the Fresnel number, N_f, given by Equation 3-1:

$$N_f = \frac{b^2}{\lambda d},$$

(3-1)

where "b is the largest radial distance within the aperture" (Saleh and Teich, 1991). In the case of $N_f \ll 1$ then the Fraunhoffer approximation is used to describe the diffraction pattern. When $N_f \gg 1$, as is the case with this spectrometer, the Fresnel approximation is

used; the diffraction pattern is the geometrical shadow of the aperture. (Saleh and Teich, 1991) The data were taken using a slit width of 600 µm and slit height of 12 mm. For a distance d to the grating of 120 mm and a maximum usable wavelength of 1200 nm N_f is 10^3.

When light strikes a grating at normal incidence it is diffracted at an angle given by Equation 3-2:

$$\sin(\theta) = \frac{n\lambda}{2d},$$ (3-2)

where d is the grating spacing (Whiffen, 1966). Each wavelength can be reflected at more than one angle. The value of n, an integer equal to 1,2,3 etc., is the order of the reflected light for a given wavelength. A filter was used when the data was collected for the bands centered at .715 µm and above to prevent interference from the higher order terms of the shorter wavelengths.

The MultiSpec™ II has a focal length of 120 mm and an effective aperture of F/3.7 (Oriel,1994). Since this gives an aperture that is greater than the slit size, it is the slit that determines the field of view. The slit used has a field of view of 2.5 m by 0.125 meters at 25 meters, the nominal distance from the spectrometer to the targets. The slit was oriented vertically.

The data consist of relative reflectance values versus wavelength and were collected for five wavelength bands centered around .425 µm, .575 µm, .715 µm, .845 µm and .950 µm. The spectrograph would be set for the desired band and three shots would be made. One would be the target, one a two percent reflecting disk, and one a 50 percent reflecting disk. The data from the known two and fifty percent reflecting disks were used by the computer for calibrating the instrument and to calculate the relative reflectance values of the target. The spectrograph was then adjusted for the next wavelength band. A filter was used in the longer wavelength bands to prevent interference from shorter wavelengths. The lighting conditions often varied during the data collection from one band to the next because of the time required to adjust the

spectrograph; however, care was taken to ensure that the lighting was essentially the same for the three shots at each band.

There was some overlap of wavelengths between bands and this allowed for manual correction of the differences caused by lighting. Also, the data at the extremes of the detector array's spectral response tended to be noisy. This noise can be eliminated with fourier filtering without adversely affecting the general shape of the overall spectrum.

B. LINEAR MIXING

Spectral mixing is a consequence of the mixing of materials within the volume of the Earth's surface associated with a single Instrument Field of View (IFOV). This thin volume is bounded in two dimensions by the pixel size and in the third by the depth of penetration of photons that escape and are recorded as reflected radiance. The aim of this analysis was to take individual "pure" endmember spectra and linearly combine them to match the observed spectrum of the scene. An endmember is one of the basis spectra that are combined to build up the total spectrum of the scene. Ideally a "pure" endmember is one in which the recording instrument's field of view did not contain any other objects. A "non-pure" endmember is one in which the field of view was not small enough to limit the spectrum to the reflectance of the object. The underpinning premise for the theory is that spectral mixing within a single pixel of the observed radiance is a result of the spatial mixing of the materials in the scene. This method rests on the assumption that the observed spectral radiance may be modeled as a linear combination of members of a "pure" endmember spectral mixing library. Figure 13 is a graphical representation of the process. The goal is then to determine the correct endmembers that are contributing to the observed spectrum and the fractional abundances of each. (Boardman, 1990)

Variations in lighting geometry affect absolute brightness (shade and shadow) and also may change spectral reflectance by altering curve slopes and shapes of bands. To

compare image spectra with reference spectra of an endmember library, it is essential to separate spectral changes due to differences in lighting geometry, illumination intensity, instrumental calibration, and atmospheric absorption from those caused by differences in surface materials. The spectral reflectance of a surface at maximum brightness can be considered as an end-member if there is a continuum of possible reflectances that range through intermediate levels of illumination to pure shadow where the illumination is zero. Zero illumination at all wavelengths is also a spectral end-member. By allowing the "shade" endmembers to mix with other endmembers, the identity of a material can be maintained throughout a scene regardless if the illumination is constant or not. This method also removes the ambiguity of secondary illumination which is not discussed here. (Adams *et al.*, 1986) "Shade" endmembers were not incorporated into this analysis.

This analysis used a constraining boundary condition in which the abundances were forced to be positive and to sum to unity.

An example of one of the equations used is:

$$\begin{bmatrix} A & B & C & D \end{bmatrix} * \begin{bmatrix} CAR(\lambda) \\ CAMO(\lambda) \\ BUSH(\lambda) \\ GRASS(\lambda) \end{bmatrix} = SCENE(\lambda) , \qquad (3\text{-}3)$$

where A, B, C and D represent the spectral abundances that multiply with the endmembers to produce a match to the observed spectrum from the combined scene. The λ is used to indicate the spectral terms that are a function of wavelength. The closest match was found using a computer algorithm written in Research Systems Inc. Interactive Data Language (IDL®). The program varied the abundaces of each endmember and then chose the abundances that minimized the RMS error between the original scene's observed spectrum and the best-fit calculated linear combination spectrum. This

minimum RMS error is referred to as the RMS minimum. The RMS error was defined as:

$$\text{RMS ERROR} = \sqrt{\frac{1}{N}\sum_{i=1}^{N}(x_i - \bar{x})^2} \; . \qquad (3\text{-}4)$$

The number of elements in the spectrum is represented by N, the relative reflectance of the calculated spectrum minus the relative reflectance of the scene at single specific wavelength is x_i, and the mean of the differences over the spectrum is $\bar{x}$. Since the reflectance is given as percent relative reflectance, the RMS error is a percent. A high RMS error value indicates that there is an insufficient number of endmember spectra in the library. When this method is used with imaging spectrometers, the error could be localized to a region of the image where the endmember is missing. For this analysis, the output of the program can be used as a final result or as a clue to the selection of a more appropriate endmember library.

C. DESCRIPTION OF CAMOUFLAGES AND CAR

Data were collected for five different camouflage nets provided by Radian Inc. to the Kestrel corporation for use in testing. These nets are various manufacturers' entries for Pre-Production Qualification Testing (PPQT) for the Army's proposed Ultralightweight Camouflage Net Systems (ULCANS). ULCANS will provide visual, electrooptic, radar, and infrared signature reduction characteristics. At the time of writing the nets were not type classified and not in the Army's inventory system. Because these nets are not yet owned by the United States Government, when the results of any testing is combined with the names of the manufacturers of these nets the information is proprietary in nature. To avoid this, the nets are referred to as camouflages one through

27

five as described below. The car and camouflage #5 and the cushman and camouflage #2 are shown in Figures 14 and 15 respectively.

- Camouflage #1. Olive green with cut flaps to create 3-D look.

- Camouflage #2. Same 3-D cut as #1 but in a desert sand color.

- Camouflage #3. Smooth 1-D uniform green net.

- Camouflage #4. Smooth 1-D uniform net in green with darker green waves in the pattern.

- Camouflage #5. Smooth 1-D uniform net in green with dark green, brown, and black waves in the pattern.

The purpose of the ULCANS is to provide concealment of Army aircraft and ground equipment when tactically deployed. It will be designed to provide visual, electro-optic, radar, and infrared signature reduction characteristics equal to the Army's current Lightweight Camouflage Screen System.

These nets were draped over a green Ford Taurus automobile and a white Cushman cart for the data acquisition. The car was parked in front of a bushy green background with a grassy foreground that had some sandy bare spots in it. The Cushman was parked in a prevalently grassy foreground and background with some bushes and mixed forest in the distant background.

This data was collected primarily during the month of June 1994 in conditions that ranged from very sunny to completely overcast.

D. MAYAN RUINS AND SHIP DATA

Data was also taken of shrimp boats in a calm ocean and Mayan ruins in a dense mixed forrest. This data is presented and briefly discussed in Appendix B.

IV. ANALYSIS

A. PRELIMINARY WORK

Each spectrum was received as a set of five data files corresponding to the five wavelength bands set into the spectrograph. The first step of the analysis was to combine these files and plot them as one spectrum with a wavelength range from .35 to just past 1.0 µm. At this point it was evident that both noise at the extremes of the spectra and illumination variation offsets between bands would have to be corrected. The illumination variation was handled by applying a offset factor to the required bands to allow the file to plot as one continuous spectrum. The noisy regions at the spectral extremes (.35 µm and 1 µm), were handled in two ways. The first solution was to simply exclude the spectra in the noisy regions. The second technique was to apply a low pass filter to the spectra and then use the entire wavelength range for comparison. Figure 16 is an example of a spectrum with the noisy areas excluded. Figure 17 shows the five camouflage scenes with the car plotted with variable offsets so that each curve is visible. The five camouflage scenes for the cushman are shown in Figure 18. Figure 19 shows the spectra for each of the camouflages alone. Figure 20 contains the car and cushman spectra and Figure 21 contains the bush and grass curves. Figures 17 through 21 all apply offsets to successive curves to allow for direct comparison.

The analysis was run with successively larger numbers of endmembers contributing to the linear combination. The filter technique was only applied to the four endmember case in this analysis.

B. CORRELATION COEFFICIENTS

A simple useful tool for comparing two or more data sets is the correlation coefficient. This is especially easy to do in IDL®. One line of code will return a value

between negative one and one. A value of one corresponds to the curves being perfectly correlated. A zero corresponds to completely uncorrelated. A negative number indicates anti-correlation which a minus one would be indicative of a mirror image. Table 1 shows how well correlated the observed spectrum is to the endmembers.

	Car	Camo	Bush	Grass	Cush
Car	1.0000	0.9938	0.9987	0.9986	0.9975
Cush	0.9975	0.9918	0.9982	0.9953	1.0000
Bush	0.9987	0.9956	1.0000	0.9976	0.9982
Grass	0.9986	0.9938	0.9976	1.0000	0.9953
Car+camo1 scene	0.9862	0.9762	0.9781	0.9841	
Car+camo2 scene	0.9854	0.9272	0.9834	0.9904	
Car+camo3 scene	0.9975	0.9963	0.9929	0.9961	
Car+camo4 scene	0.9985	0.9891	0.9934	0.9970	
Car+camo5 scene	0.9984	0.9649	0.9939	0.9969	
Cush+camo1 scene		0.9569	0.9591	0.9674	0.9657
Cush+camo2 scene		0.9259	0.9760	0.9782	0.9763
Cush+camo4 scene		0.9632	0.9630	0.9691	0.9665

Table 1. Correlation Coefficients.

Note the high general correlation in each comparison. This is a result of the relatively large field of view of the spectrometer. Because of this large field of view, the endmembers are not "pure" but contain parts of the rest of the scene in them. Traditional analysis techniques rely on the pureness of the endmember library. While the following analysis is affected by the lack of pureness of the endmembers, it is not precluded by it.

C. TWO ENDMEMBERS

The first set of analysis was run with two endmembers, the car and the camouflage. Thus, in this case the background and foreground were ignored. Equation 4-1 is a vector representation of the logic used to calculate the linear spectral combination to be plotted and compared against the observed spectrum of the scene.

$$\begin{bmatrix} A & B \end{bmatrix} * \begin{bmatrix} CAR(\lambda) \\ CAMO(\lambda) \end{bmatrix} = \text{LINEAR COMBINATION}(\lambda) \qquad (4\text{-}1)$$

The sum of the abundances A and B is restricted to unity or less. In this analysis the abundances are also constrained to be positive. With pure endmembers, positive abundances are the only case that have physical meaning. If the endmembers are not pure, then negative abundances have meaning. In the non-pure endmember case, the endmembers may redundantly contain the same parts of the scene. For example, the car endmember still has the grass foreground and the bushy background in it; the bush endmember still has the grass in it; and the grass endmember still has bush in the scene. Additionally, the scene contains a fair amount of visible sand for which there was no endmember. A demonstration of an unconstrained run will be shown for the four endmember runs.

The linear combination spectrum is anchored to the observed spectrum to force the comparison to be more one of shape rather than relative amplitude. As Table 2 shows, the anchor point does affect the results. Runs were conducted with three endmembers for the car and camouflage #1 data set successively at anchor points of .42, .54, .68, and .78 μm.

31

Anchor (μm)	A	B	C	RMS min
0.42	0.00	0.55	0.45	2.00
0.54	0.39	0.46	0.15	2.25
0.68	0.58	0.27	0.15	1.65
0.78	0.78	0.22	0.00	1.77

Table 2. Results on abundances due to varying the anchor point.

For the analysis, an anchor point of .42 was chosen. By choosing an anchor point that occurs before the distinguishing features of the spectrum, it can better be determined how different endmembers are affecting these features. The results of the two endmember runs are summarized in Table 3.

Data Set	A	B	RMS MIN
car and camo1	0.62	0.38	2.73
car and camo2	0.60	0.40	2.53
car and camo3	0.99	0.01	4.10
car and camo4	0.99	0.01	2.77
car and camo5	0.99	0.01	1.39
cushman and camo1	0.28	0.72	2.50
cushman and camo2	0.77	0.23	1.12
cushman and camo3	no data	no data	no data
cushman and camo4	0.49	0.51	3.11
cushman and camo5	no data	no data	no data

Table 3. Summary of two endmember runs for all data sets.

There are some similarities in the runs with the car. Excluding the run with camouflage #4, all linear combination best fit curves have a shallower slope than the observed scene on the infrared ledge. These four linear combination curves also plateau in the near infrared at a lower relative reflectance than the observed scenes. In the visible and, specifically, at the green peak at approximately .54 μm, the runs with camouflages #1, #3,

and #5 are similar. In these three curves, the linear combination's green peak is considerably less than the observed spectrum's in relative amplitude. The best fit for the car and camouflage #3 data set is shown in Figure 22.

For the observed spectrum containing the entire scene for the cushman and camouflage with camouflage numbers three and five, the data recorder did not record reflectance data for the band centered at .845 μm. Although the rest of the spectrum is present, this absence of data prevents proper analysis of these data sets.

D. THREE ENDMEMBERS

The second set of runs for the car data sets added the bushy background as a third endmember. The cushman set of data did not have the exact same background as the car data set. The cushman set used grass as the third endmember background. Equation 4-2 is a vector form of the equation used to compute the linear combination for the car:

$$\begin{bmatrix} A & B & C \end{bmatrix} * \begin{bmatrix} CAR(\lambda) \\ CAMO(\lambda) \\ BUSH(\lambda) \end{bmatrix} = \text{LINEAR COMBINATION} \tag{4-2}$$

Again, the sum of the abundances was required to be unity or less. The anchor was set at .42 μm. With three endmembers the computer algorithm initially generated a family of curves each showing a different bush abundance. The minimum RMS value was then picked from this family. In general, the effect of increasing the abundance of bush in the linear combination has the effect of increasing the slope of the infrared ledge. Table 4 is a summary of the best fit curves for the different data sets.

The best fit for the car and camouflage #3 (see Figure 23) showed a dramatic reduction in the RMS minimum by 2.98 down to 1.12. There was improvement over the two endmember run throughout the entire wavelength range. The three endmember

combination's only "weak point" is that it is about 1% too high in the .58 to .65 μm wavelength range.

For the cushman data sets, grass was added as the third endmember. When the third endmember was added to the cushman and camouflage #1, the RMS minimum was decreased by only .34 to 2.16. Overall, this linear combination is not a very good match to the observed scene but improvements were made over the two endmember case. The three endmember run for the cushman and camouflage #2 improved the RMS minimum by only .14 to .98. This time the improvement was over an already good match and the result is a very good fit to the observed spectrum. As with the previous two data sets, the addition of grass to the cushman and camouflage #4 data set only marginally improved the RMS minimum. Additionally, the improvements came in the same wavelength ranges as the previous two data sets. The peak of the green hump and its downslope were slightly improved as well as the slope of the infrared ledge increasing to slightly greater than that of the observed scene. Another similarity is that the two and three endmember curves are identical from .4 to .5 μm for all three cushman data sets.

Data Set	A	B	C	RMS MIN
car and camo1	0.00	0.55	0.45	2.00
car and camo2	0.26	0.29	0.45	1.55
car and camo3	0.06	0.49	0.45	1.12
car and camo4	0.99	0.01	0.00	2.77
car and camo5	0.45	0.25	0.30	0.62
cushman and camo1	0.32	0.23	0.45	2.16
cushman and camo2	0.67	0.18	0.15	0.98
cushman and camo3	no data	no data	no data	no data
cushman and camo4	0.17	0.08	0.75	2.71
cushman and camo5	no data	no data	no data	no data

Table 4. Summary of three endmember runs for all data sets.

E. FOUR ENDMEMBERS

The third run added the grassy foreground to the car data sets and added some bush background to the cushman data sets. Equation 4-3 represents the equation used to compute the linear combinations for the car data set:

$$\begin{bmatrix} A & B & C & D \end{bmatrix} * \begin{bmatrix} CAR(\lambda) \\ CAMO(\lambda) \\ BUSH(\lambda) \\ GRASS(\lambda) \end{bmatrix} = LINEAR\ COMBINATION. \qquad (4\text{-}3)$$

The sum of the abundances was restricted to unity or less and the spectra were anchored at .42 μm. The best fit curves for run three are summarized in Table 5. The best fit for the car and camouflage #3 is plotted in Figure 9. Only the car and camouflages #2 and #3 were improved by the addition of grass as a fourth endmember. With the car and camouflage #2, the addition of grass decreased the RMS minimum by .07 to 1.48. The abundances of the camouflage and the bush did not change but the car abundance decreased by .14 and the grass abundance was .15. Overlaying the three and four endmember curves reveals no detectable difference in shape or magnitude.

The four endmember best fit for the car and camouflage #3 (see Figure 24) had an improvement in the RMS minimum by only .01. The abundance of the bush was unchanged and the abundance of the car went to zero. Again, the improvement to the curve is not visible by overlaying the curves.

An unconstrained run where the abundances were not restricted to positive values was done for the car and camouflage #4 set. In the constrained case the RMS minimum was 2.77 with the abundances: A=.99 and B=.01. The RMS minimum for this

35

The best fit linear combination for all data sets with the cushman had a zero abundance of bush in them. Thus the best four endmember solution is the same as the best three endmember solution for each set.

It is appropriate at this point to note that when comparing Table 5 to Table 1, the most correlated endmember did not necessarily correspond to the highest abundance. There are however, similarities and as a general rule the correlation coefficient for the scene to the linear combination did improve in conjunction with an improvement in the RMS minimum.

Data Set	A	B	C	D	RMS MIN
car and camo1	0.00	0.55	0.45	0.00	2.00
car and camo2	0.12	0.28	0.45	0.15	1.48
car and camo3	0.00	0.40	0.45	0.15	1.11
car and camo4	0.99	0.01	0.00	0.00	2.77
car and camo5	0.45	0.25	0.30	0.00	0.62
cushman and camo1	0.32	0.23	0.45	0.00	2.16
cushman and camo2	0.67	0.18	0.15	0.00	0.98
cushman and camo3	no data	no data	no data	no data	no data
cushman and camo4	0.17	0.08	0.75	0.00	2.71
cushman and camo5	no data	no data	no data	no data	no data

Table 5. Summary of four endmember runs for all data sets.

F. LOW PASS FILTER RESULTS

The spectral response of the InstaSpec™ II detector array is .180 to 1.100 μm; however, the data at the extremes of this range have quite a bit of high frequency noise. Some of the noise was eliminated by setting the data points that were negative to zero. Those data that were recorded as "not a number" were deleted. This still left quite a bit of oscillation in the extremes. In an attempt to see if the noise had a significant affect on the

results, the data were fourier transformed, sent through a low-pass filter, and then inverse transformed. The filtered data was then combined in the manner previously described. Since the data for the bush had only the first four bands available, only the first four bands of the data sets were used. The plotted results for the car combined with camouflage #3 are in Figures 26 and 27. Figure 27 is the result for excluding the noise in the analysis. The solid line is the filtered scene. The dash-dot line is the filtered combination and the dotted line is the unfiltered combination. The unfiltered combination results printed in the lower right of each plot are from comparison with the unfiltered scene.

With the exception of the car and camouflage #4, all of the RMS minimums for the filtered data are less than that for the unfiltered data when the data below .400 μm is used. It should be noted that the RMS values for the unfiltered data calculated in these runs were different than those calculated in the earlier runs using the same abundance values. The difference is not consistently higher or lower and most likely results from the way the data arrays were resized after removal of the bad data points.

When the data below .400 μm is removed the abundances for both the filtered and unfiltered combinations changes, as does the difference between RMS minimums. In this case the unfiltered minimums are greater than the filtered minimums for all but the car and camouflage #2 where the filtered minimum is a full point greater. Again the values calculated here for the unfiltered data differ from the minimums calculated earlier. The majority of the summary below is for the filtered data which includes the values below .400 μm.

Using the car and camouflage #1, calculations were made using the unfiltered abundances for both, the filtered abundances for both, and changing the anchor point but not the abundances to see if these changes affected the RMS values or their relation to one another. When the same abundances were used for both the filtered and unfiltered combinations, the filtered RMS value remained less than the unfiltered value; even though, the actual values did change.

37

As with the unfiltered data, the fourth endmember, the bush, was zero for the cushman combinations with camouflages 1, 2, and 4. The combinations of the cushman with camouflages #3 and #5 were not available due to missing data bands.

For the cushman with camouflage #1 the abundances for the filtered combination were almost exactly the same as for the unfiltered case yet the RMS minimum is almost 2 points lower. The two combinations plot almost on top of one another with the unfiltered line being slightly higher at the plateau. The peak in the green is also slightly higher in the unfiltered result. There are three distinct dips in the plateau of the filtered scene. These dips are also present in the filtered combination although they are not as deep or distinct. The presence of the noise makes these dips less distinct in the unfiltered versions and may account for some of the difference in the RMS values between the filtered and unfiltered data. When the noisy data below .400 μm is deleted, the abundances for the filtered and unfiltered become significantly different from one another, but the RMS minimum for the unfiltered case is slightly less than 1 point greater.

In the case of camouflage #2 and the cushman the filtered and unfiltered abundances are different. The filtered combination uses less of the cushman endmember, 67 percent to 51 percent, but more of the grass endmember, 15 percent to 31 percent. Both combinations use the same amount of the camouflage endmember. Both combinations start at about the same reflectance levels but the filtered combination begins to have a higher value beginning at about the .40 μm point. The filtered combination also follows the slope of the infrared ledge more closely, and the value at the plateau is much closer to the scene than is the unfiltered combination. Again there are three distinct dips in the plateau of the scene, although the dips can be seen in both the filtered and unfiltered combinations on this run. When the noise at the beginning is removed, the RMS minimum for the filtered combination increases while it decreases for unfiltered combination, although the unfiltered value is still 0.7 greater than the filtered value.

As with camouflage one, the abundances for camouflage #4 and the cushman are almost identical in the filtered and unfiltered combinations. In this instance the difference

in RMS minimums is almost 2.5. The unfiltered reflectance value is ever so slightly less in the visible region and essentially identical with the filtered data beyond .650 μm. Again when the data below .400 μm is removed the abundances change. At 1.5, the difference between the RMS minimums is a full point less than the previous value.

The car and camouflage #1 plots for the filtered and unfiltered case are quite similar although the abundances are not. The filtered combination follows the scene more closely in the range from .450 to .500 μm and the filtered plot peaks slightly higher around .525 μm. Beyond .550 μm the filtered and unfiltered plots are essentially identical although the unfiltered plot has a slightly steeper slope towards the plateau. The filtered combination uses 49 percent car endmember while the unfiltered uses none. On the other hand, the filtered combination uses only 7 percent of the grass endmember while the unfiltered combination uses 60 percent. Using the filtered abundances on the unfiltered files increases the unfiltered RMS value slightly, from 3.84 to 3.93. The change in the filtered RMS value when using the unfiltered abundances is also small, from 2.93 to 3.15. When the noise below .400 μm is removed, the filtered RMS value and abundances change very little. The values for the unfiltered change quite a bit and the RMS minimum is actually greater in this case than with the noise included.

When camouflage #2 is mixed with the car the plots are very similar to the actual scene plot. The combinations start out slightly less than the actual scene. All three have a sharp peak around the .500 μm point where the values are approximately the same dropping slowly to a minimum just beyond .650 μm. The infrared ledge of the three plots is again essentially the same although at the plateau the unfiltered plot is less than the scene and the filtered combination which are essentially the same. The significant difference between the two combinations is the abundances of grass, bush, and car endmembers. The filtered combination uses very little grass, only 3 percent, while the unfiltered combination uses ten times that. The unfiltered combination uses no car endmember and 45 percent bush. The filtered combination uses 66 percent bush and 4 percent car endmembers. The RMS difference is slightly greater than 2. When the data

below .400 μm is removed the filtered and unfiltered combinations trade places. The unfiltered combination is much closer to the actual scene and has the lower RMS minimum.

The car mixed with camouflage #3 in statistically identical abundances for the filtered and unfiltered cases, and the two plots are identical except for the noise in the unfiltered plot. The difference between the RMS minimums in this case is the closest of the eight instances. The filtered result is only 0.7 less than the unfiltered result, and the combinations very closely resemble the scene. Below about .500 μm all three plots are the same. The scene peaks higher around 550 μm, but the general shape of the curves is the same through .650 μm. Just beyond .650 μm the minimum for the scene is slightly less than the combinations; however, all three begin and end the infrared ledge at the same time. The scene has a sharper turn onto the plateau but the average value of the plateau is very close for the scene and the combinations. Although the abundances for the filtered and unfiltered combinations are no longer the same when the data below .400 μm is deleted, the two curves are still quite similar and the difference in RMS minimums is 0.4.

The closest fit is achieved with the car and camouflage #5. The RMS value for the filtered case is just less than one and just less than three for the unfiltered case. These quite similar plots were again achieved using significantly different abundances. Where the filtered combination is mostly car endmember with no grass, the unfiltered case is mostly grass endmember with only one percent car. The abundances for camouflage and bush were approximately the same for both combinations. Below .500 μm the filtered combination more closely follows that of the scene. It has the same general shape and slope; whereas, the unfiltered combination begins by rising more sharply and then turning to a more shallow slope to finish at a lower value. Beyond .500 μm the curves all follow the same general shape. The scene is much higher at the peak near .575 μm but all three drop to approximately the same minimum near .700 μm and beyond that are the same. The two curves are still quite similar to the scene when the data below .400 μm is

removed; however, the abundances for the unfiltered combination changed significantly. The RMS minimum for the filtered combination remained just less than one while the minimum for the unfiltered scene is 1.4, about half of its previous value.

Camouflage #4 presented some unusual results when filtered and mixed with the car. The minimum RMS value is achieved with only one endmember, the car. Unlike the other plots which anchored at the .400 μm point, this set is anchored at the minimum for the scene, near .675 μm. All three plots are similar beyond the anchor point except for the step in the plateau for the scene which is not seen in the combinations. Below the anchor point there are significant differences. The scene has a much higher value throughout the lower wavelengths until it drops sharply near .600 μm. All three plots peak in the vicinity of .525 μm, but the slope up to that peak is much steeper for the combinations than for the scene. This remains true whether or not the data below .400 μm is used.

V. DISCUSSION

A. PATTERNS IN THE DATA

There are some fairly consistent patterns that are evident from the data. Chapter IV organizes the data in three runs (two, three, and four endmembers), each with eight cases (the car with camouflages one through five and the cushman with camouflages one, two, and four). The following sections discuss patterns for both cases and runs.

1. Patterns within Runs

Referring to Table 2, data for the two endmember runs, it can be seen that the car dominates each of its data sets. For camouflages #3, #4, and #5 the abundance for the car is .99. The cushman does not dominate each of its data sets. The mean abundance for the car or cushman was .72 versus .28 for the camouflage. In general, the two endmember run's abundances do not appear to be realistic.

For the three endmember runs, refer back to Table 3. For the car and camouflage #1, #2, and #3 the bush contributes .45 to the linear combination. In data set #5 it contributes .3. Also in camouflages #1, #2, and #3 the car is the least abundance. For camouflages #4 and #5 the car abundance is the highest. As in the two endmember runs, there are no real patterns in the cushman data sets for this run. These abundances are seemingly more realistic. The car and camouflage #4 was made to look more meaningful by allowing the abundances to have negative values.

The four endmember runs are summarized in Table 4. In all cases with cushman data sets, the addition of the fourth endmember (the bush) did not affect the best fit curve. The bush abundance was zero and the other abundances were identical to the three endmember case. For the car data sets, only in camouflages #2 and #3 did the fourth endmember (grass for the car) improve the linear combination. For both of these data sets the abundance for the grass was .15.

43

2. Patterns within Cases

Table 6 is a reorganization of Tables 2 through 4 to present the data for this section. The correlation coefficient is also included in the last column. This is the coefficient for the linear combination compared to the observed spectrum of the scene. In the car and camouflage #1 data set, the addition of the bush improved both the minimum RMS value and the correlation coefficient. Starting with the three endmember run where background was added in, the car made no contribution to the linear combination. This is despite the fact that the car spectrum was the most highly correlated to both the linear combination and the observed spectrum. The fourth endmember grass made no contribution when it was added in.

The RMS minimum improved with the addition of the bush and the grass for the car and camouflage #2. The correlation coefficient was highest for the three endmember best fit solution. The bush endmember abundance was .45 in the three endmember run and remained at .45 with the addition of grass for the four endmember run.

Similar to the previous run the car and camouflage #3 data set improved its RMS minimum with each of the three runs and its correlation coefficient was highest at the three endmember case. The abundance for the car which dominated at .99 for the two endmember case went to .06 and then to zero with the addition of the bush and grass respectively. Also like the previous data set, the bush abundance remained at .45 before and after the grass was added in. The grass contributed .15 for both of these data sets.

The car and camouflage #4 data set did not change with the addition of the bush or grass. The car abundance dominated at .99 for all runs.

The car and camouflage #5 data set was the only car data set that the car remained dominant when there were contributions from the background. The grass did not contribute to the combination.

44

Data Set/endmembers	CAR	CAMO	BUSH	GRASS	RMS	CORR
Car and camo #1/two	0.62	0.38			2.72	0.9931
/three	0	0.55	0.45		2	0.994
/four	0	0.55	0.45	0	SAME	SAME
Car and camo #2/two	0.6	0.4			2.53	0.9904
/three	0.26	0.29	0.45		1.55	0.9956
/four	0.12	0.28	0.45		1.48	0.9943
Car and camo #3/two	0.99	0.01			4.1	0.9973
/three	0.06	0.49	0.45		1.12	0.9978
/four	0	0.4	0.45	0.15	1.11	0.9974
Car and camo #4/two	0.99	0.01			2.77	0.9983
/three	0.99	0.01	0		SAME	SAME
/four	0.99	0.01	0	0	SAME	SAME
Car and camo #5/two	0.99	0.01			1.39	0.9983
/three	0.45	0.25	0.3		0.62	0.9985
/four	0.45	0.25	0.3	0	SAME	SAME
Cush and camo #1/two	0.28	0.72			2.5	0.9619
/three	0.32	0.23		0.45	2.16	0.9743
Cush and camo #2/two	0.77	0.23			1.12	0.9789
/three	0.67	0.18		0.15	0.98	0.9884
Cush and camo #4/two	0.49	0.51			3.11	0.9655
/three	0.17	0.08		0.75	2.71	0.9697

Table 6. Summary of abundances.

In the cushman data sets, since there are only two runs to compare (the four endmember abundances were identical to the three endmember abundances), it is more difficult to establish patterns. It is noted however, that both the RMS minimum and the correlation coefficient improved for all three runs with the addition of the grass to the linear combination. In the cushman and camouflages #1 and #4, the grass was the highest abundance of the combination.

3. Natural Versus Man-made Materials

In addition to patterns within the runs and cases, patterns in the relative percentages of man-made and natural abundances contributing to the scene were analyzed. Table 7 summarizes this data. In the table the sum of the man-made abundances (the car and camouflage) is abbreviated "man," and the sum of the natural abundances (the grass and the bush) is abbreviated "nat."

	Camo #1		Camo #2		Camo #3		Camo #4		Camo #5	
	man	nat	man	nat	man	nat	man	nat	man	nat
Car	0.55	0.45	0.4	0.6	0.4	0.6	1	0	0.7	0.3
cushman	0.55	0.45	0.85	0.18			0.25	0.75		

Table 7. Comparison of man-made versus natural abundance.

For the camouflage #1 data sets, the car and the cushman sets both had the same split of .55 man-made and .45 natural contributions. Man-made abundances dominated the car and camouflages #1, #4, and #5 data sets. The data sets with camouflages #2 and #3 both had .60 natural abundances.

Man-made abundances dominated the cushman and camouflages #1 and #2 with the natural abundances dominating the camouflage #4 data set.

B. LOW PASS FILTER

In all cases the filtered files produce lower RMS minimum values whether using the same or very different abundances. This would indicate that it is important to remove noise in order to achieve a closer fit; however, filtering the noise does not result in a perfect fit. Noise, therefore, is not the only reason that the endmembers cannot be combined in this case to mimic the final scene. The noise below .400 µm is of higher amplitude than that which is between .400 and .900 µm. When it is removed altogether

amplitude than that which is between .400 and .900 µm. When it is removed altogether instead of merely filtering it away, the RMS minimums are lower indicating it would be best not to use the data at the extremes at all.

VI. SUMMARY

Field spectral measurements of five camouflaged nets were analyzed. The data used in this analysis was collected by the Kestrel Corporation using a MultiSpec™ spectrograph by Oriel. For each of the five nets a spectrum of a car, a cushman cart, a background bush, grass, and the net by itself were taken. A spectrum for the net draped over the car in front of the bush was taken as well as one with the camouflaged net draped over the cushman in a predominately grassy foreground and background. The field of view for the spectrometer was 2.5 meters in the vertical and .124 meters horizontally.

The goal of the analysis was to take individual "pure" endmember spectrums and linearly combine them to match the observed spectrum of the scene. The underpinning premise for the theory is that spectral mixing of the observed radiance is a result of the spatial mixing of the materials in the scene. Spectral mixing is a consequence of mixing within a single pixel. This method rests on the assumption that the observed spectral radiance may be modeled as a linear combination of members of a "pure" endmember spectral mixing library. The endmembers library for this analysis was the car, the cushman, a bush, and a spectrum of grass. These endmembers were not as "pure" as required by traditional techniques and as would be desired for optimum results of this analysis. This was a function of the field of view of the spectrometer contained more than just the endmember when its spectrum was taken. So the goal was to determine how each of these endmembers combined to form the observed spectrum of the scene.

The best fit was found using a computer algorithm written in Research Systems Inc. Interactive Data Language (IDL®). The program chose the abundances that minimized the RMS error between the original scene's observed spectrum and the best-fit calculated linear combination spectrum. Four different runs were performed on each of eight data sets. The first three runs were runs with two, three, and four endmembers respectively. The fourth run used a low pass filter to reduce the noise in the spectra before building the linear combination and finding a best fit curve.

These best fit abundances were then tabulated and analyzed to determine if any patterns were evident. A pattern in the data would be the first step toward establishing an exploitable parameter that could be used to unmask camouflaged targets.

The best fit solutions with the exception of the car and camouflage #4 data set, improved in both RMS difference value and correlation coefficient with the addition of the third endmember which was the most prominant background component. The addition of the fourth endmember component had little or no effect on the abundances for the four endmember runs.

In the cushman data sets, since there are only two runs to compare (the four endmember abundances were identical to the three endmember abundances), it is more difficult to establish any patterns. It is noted however, that both the RMS minimum and the correlation coefficient improved for all three runs with the addition of the grass to the linear combination. In the cushman and camouflages #1 and #4, the grass was the highest abuñdance of the combination.

Next an attempt was made to determine if man-made materials or the natural materials were dominating the linear combination. For the camouflage #1 data sets, the car and the cushman sets both had the same split of .55 man-made and .45 natural contributions. Man-made abundances dominated the car and camouflages #1, #4, and #5 data sets. The data sets with camouflages #2 and #3 both had .60 natural abundances.

Man-made abundances dominated the cushman and camouflages #1 and #2 with the natural abundances dominating the camouflage #4 data set.

Finally, a low pass filter was used to "clean up" the files in an attempt to determine if the noise in the spectra was preventing the best fit program from getting as good of a match as it could. In all cases the filtered files produce lower RMS minimum values whether using the same or very different abundances. The noise below .400 μm is of higher amplitude than that which is between .400 and .900 μm. When it is removed altogether instead of merely filtering it away, the RMS minimums are lower indicating it would be best not to use the data at the extremes at all.

VII. CONCLUSIONS

The computer algorithm used in this analysis demonstrated the potential to use linear spectral mixing and unmixing to exploit camouflaged vehicles. The task of reconstructing the observed spectra was performed with a crude, non-pure endmember library. The endmembers used in the analysis were non-pure in the sense that their spectra contained contributions from the background. Even greater success could be achieved with a more sophisticated and complete library. The key to getting pure endmembers is reducing the field of view of the spectrometer so that only the desired endmember is contributing to the spectrum collected. This would be best accomplished by reducing the range between the desired endmember and the spectrometer until the endmember completely filled the field of view. It is very important that the spectra used as endmembers be as "pure" as possible and contain only the spectrum for the endmember desired for optimum results.

The background material presented on a shade endmember could contribute greatly to this analysis. A shade endmember would account for different levels of illumination across the wavelength bands. This could eliminate the need to anchor the spectra together and would certainly eliminate the need to provide offset corrections to the spectra to get them to plot as one continuous spectrum.

The analysis of the data disclosed several exploitable patterns. A sensor can now be conceptualized that would be able to breakdown a vegetative scene into its endmembers on "the fly." Then by constantly subtracting this "background" out, anything left could be compared to an endmember threat library of military targets and known camouflaging systems. This would promptly expose the target. Such a system would, in addition to defining the endmembers present in a scene, be able to compensate for the health of the vegetation, the shade and indirect lighting of the background, and the thickness of the canopy. With all these factors considered, any spectral signature left would be classified as man made. This system should apply this techniques using as

51

advanced technology as possible, such as an imaging spectrometer, to take full advantage of both the spatial and spectral information to expose potential targets.

The wavelength range considered in this analysis should not be considered the limit to exploiting linear spectral mixing and unmixing. In addition to the distinguishing features of the green hump at .45 μm and the infrared ledge at about .7 μm it would be interesting to analyze data in the 1.2 to 2.4 μm range. In this region water absorption dominates the spectra of green plants and it is quite possible that man-made materials could be picked out of these features.

APPENDIX A. FIGURES

This appendix contains all figures referred to in the text. In the analysis plots, the solid line is the observed spectrum and the dashed line is the linear combination. The abundances for the car data sets are:

- •A = CAR
- •B = CAMOUFLAGE
- •C = BUSH
- •D = GRASS

The endmembers for the cushman data sets are:

- •A = CUSHMAN
- •B = CAMOUFLAGE
- •C = GRASS
- •D = BUSH
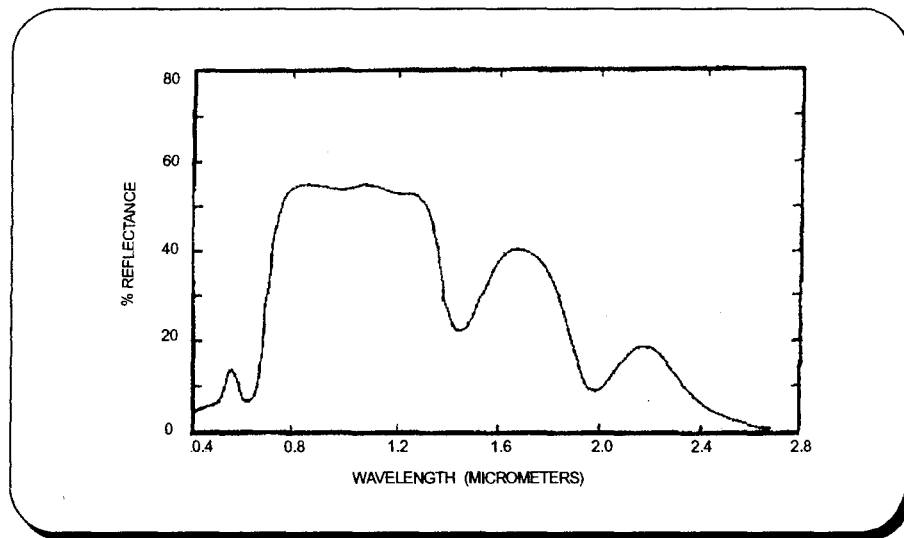
Figure 1. Typical spectrum of a green leaf. (Knipling, 1970)
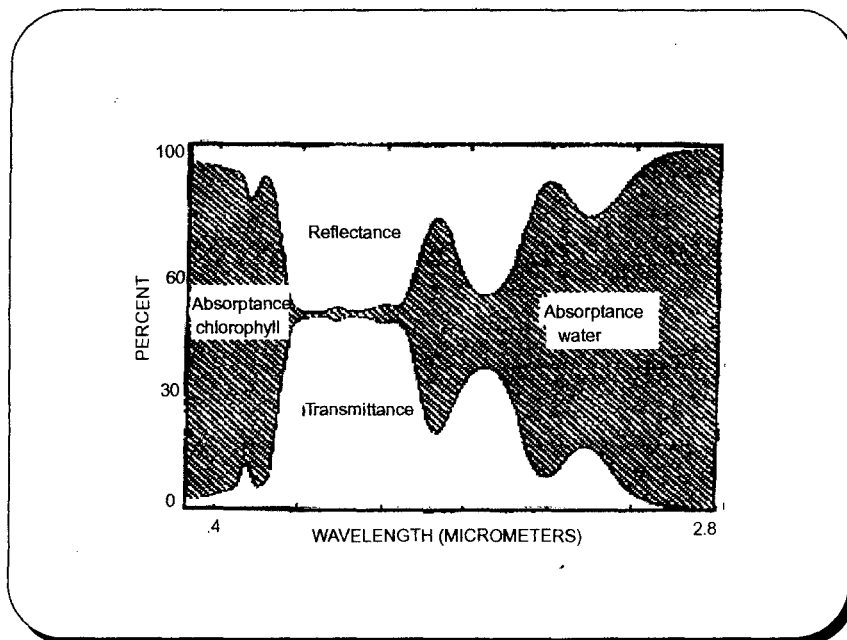
Figure 2. Reflectance, absorptance, and transmittance spectra of a plant leaf. (Knipling, 1970)
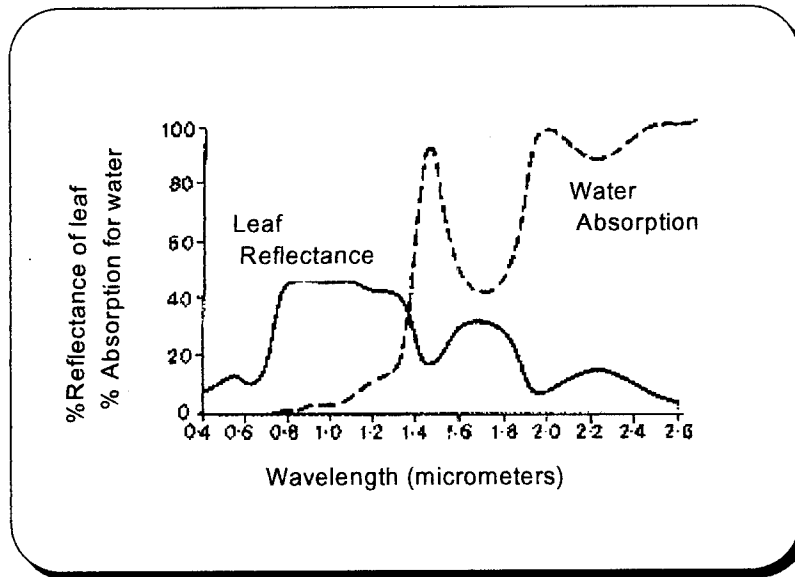
Figure 3. Leaf reflectance spectral signature showing the regions of water absorption. (Barrett, 1976)
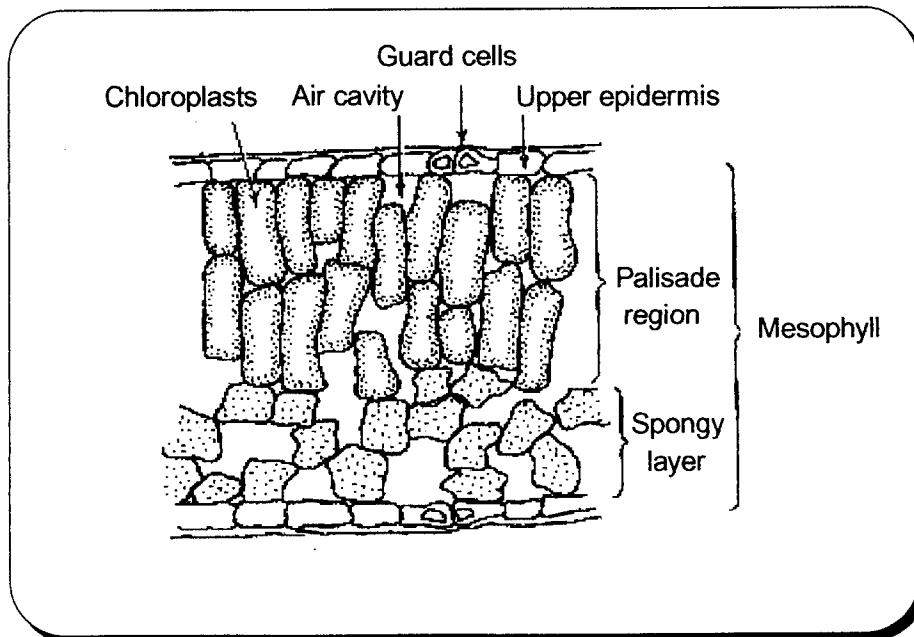
Figure 4. Cross section of a leaf. (Barrett, 1976)
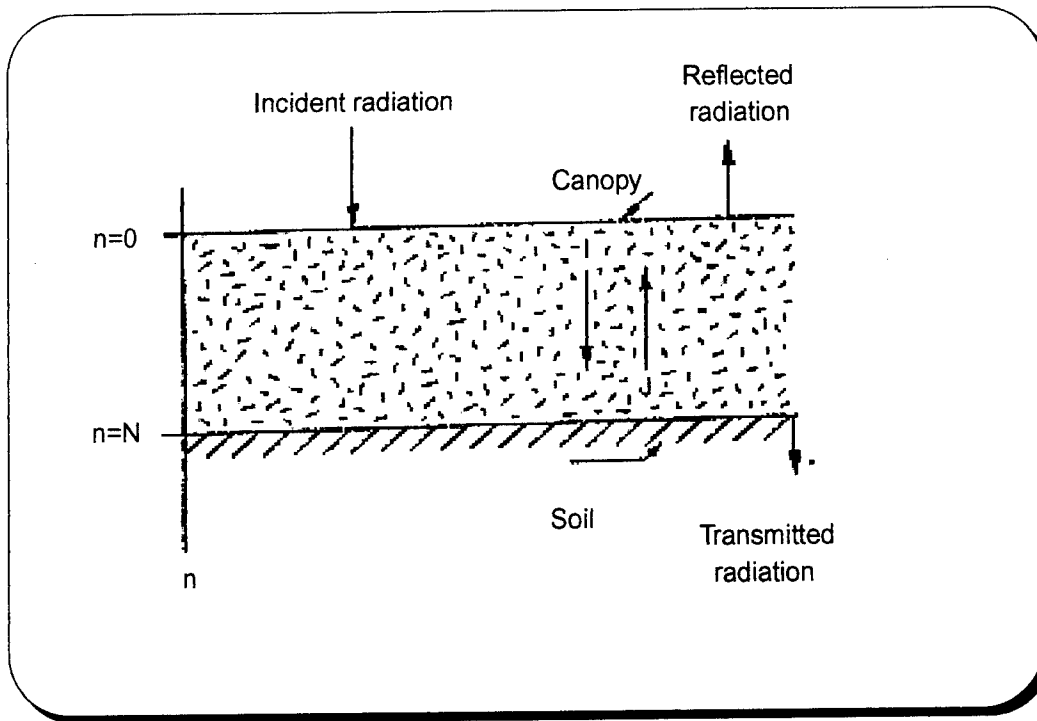
Figure 5. Geometry of a plant canopy. (Allen, 1969)
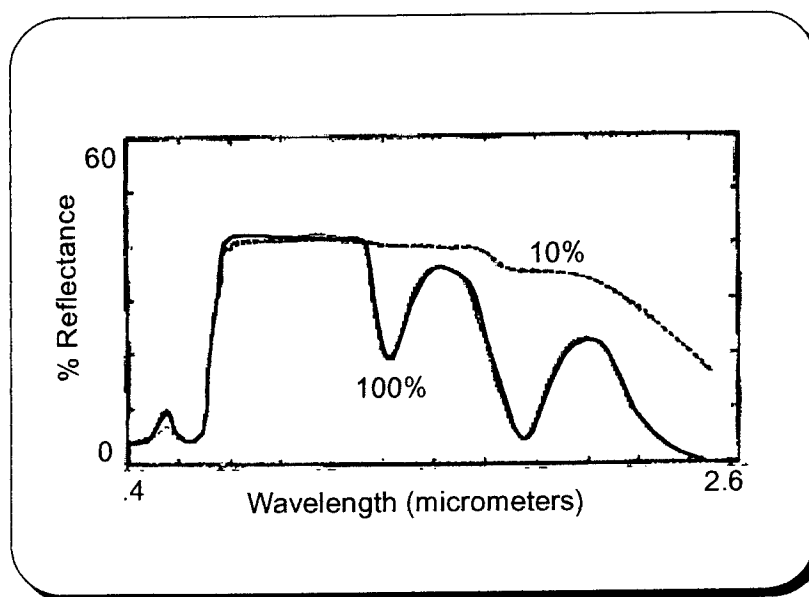
Figure 6. Effect of dehydration on leaves. 10% and 100% refer
to the water content as a percentage of their water content when
fully hydrated. (Knipling, 1970)
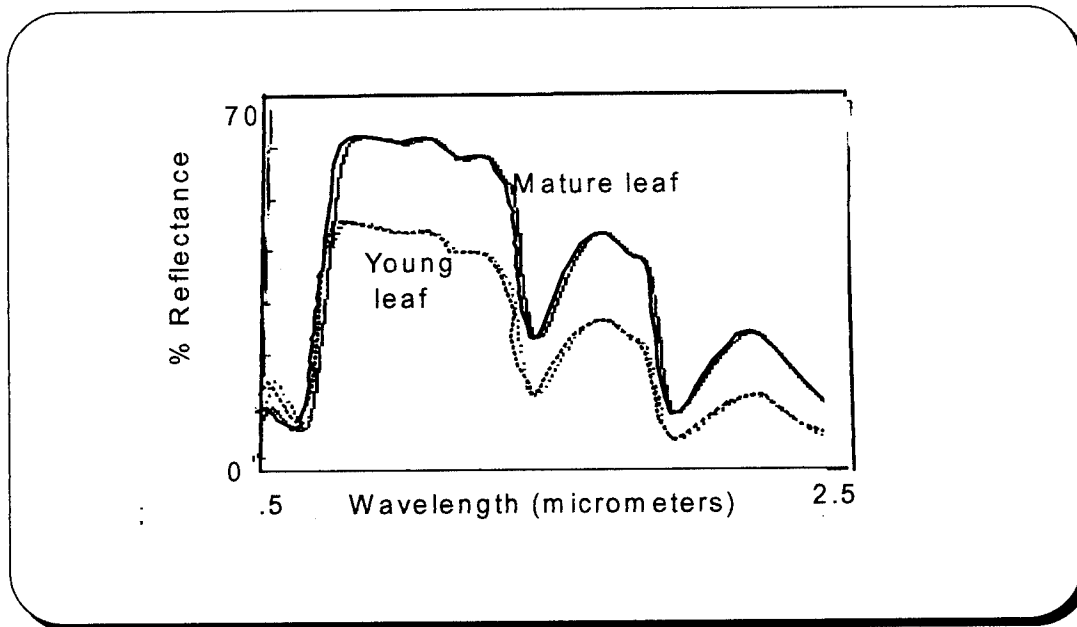
Figure 7. Comparison of reflectances of young and mature leaves. (Janza, 1975)
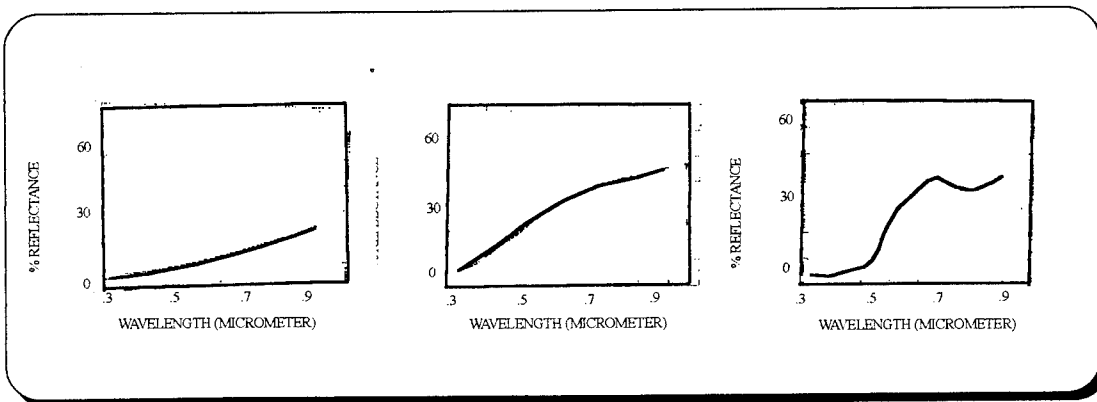
Figure 8. Characteristic spectra of Type I, Type II, and Type III soils. (Condit, 1970)

57
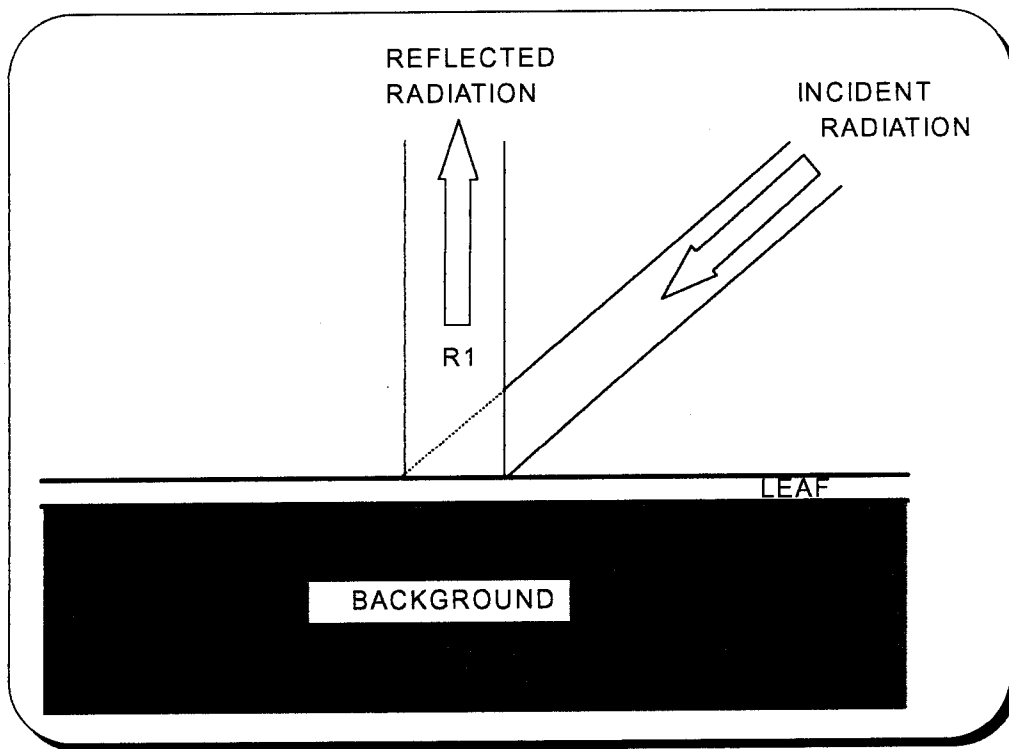
Figure 9. Single leaf on a plane background (Lillesaeter, 1982)

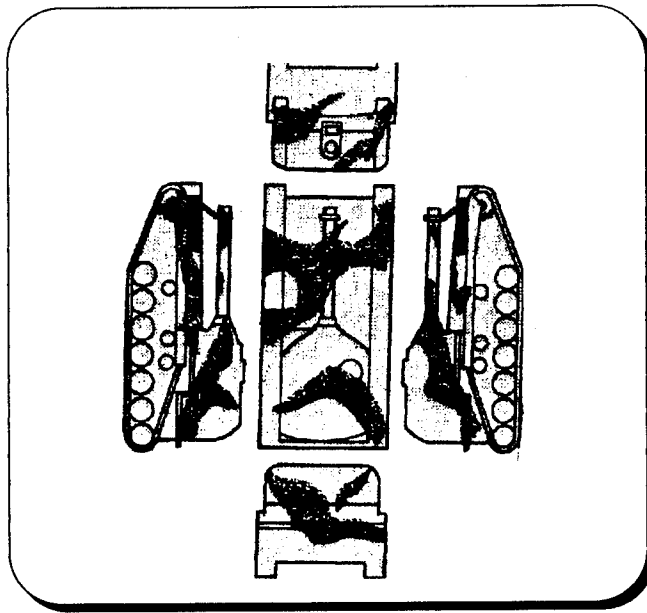SHADOW   RELATIVE POSITION   SHAPE
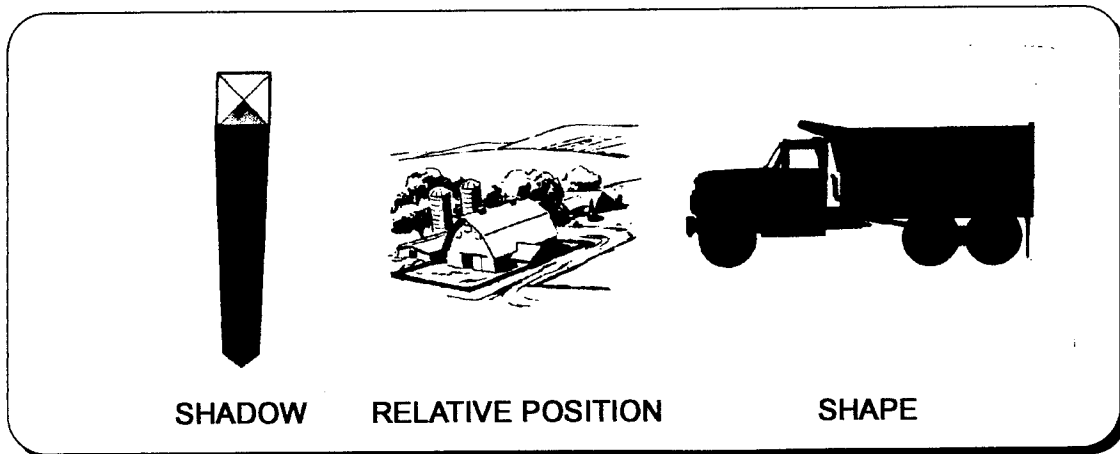
Figure 10. Factors of recognition. (Department of the Army, 1968)

Figure 11. Light and dark patterns are used to break up the appearance of straight lines. (Department of the Army, 1968)
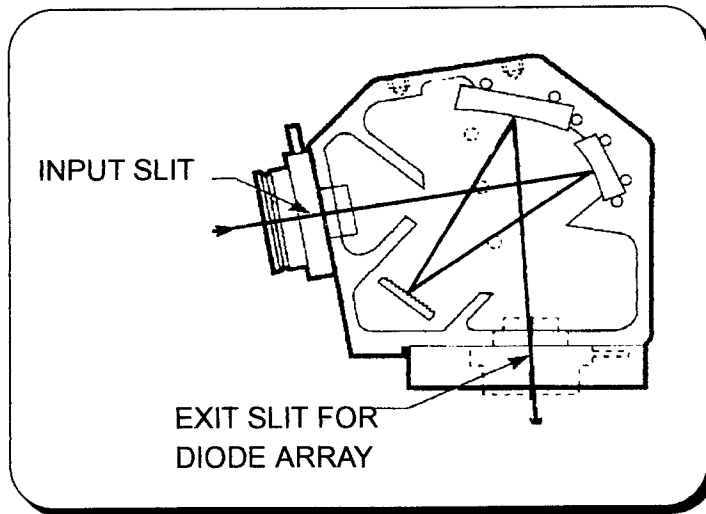

INPUT SLIT

EXIT SLIT FOR DIODE ARRAY

Figure 12. Optical configuration of spectrograph (Oriel, 1994)
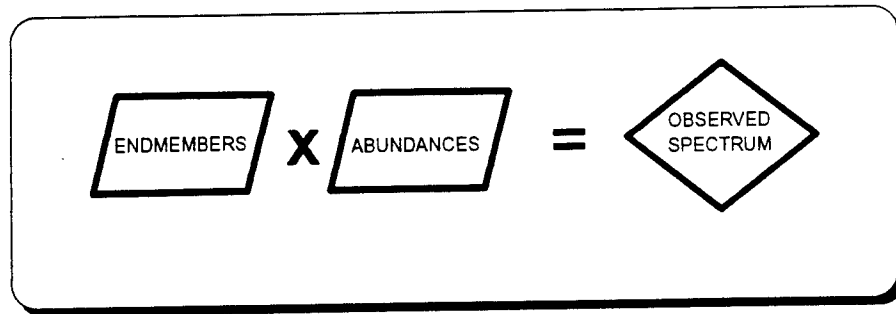
Figure 13. Linear spectral mixing. (Boardman, 1990)
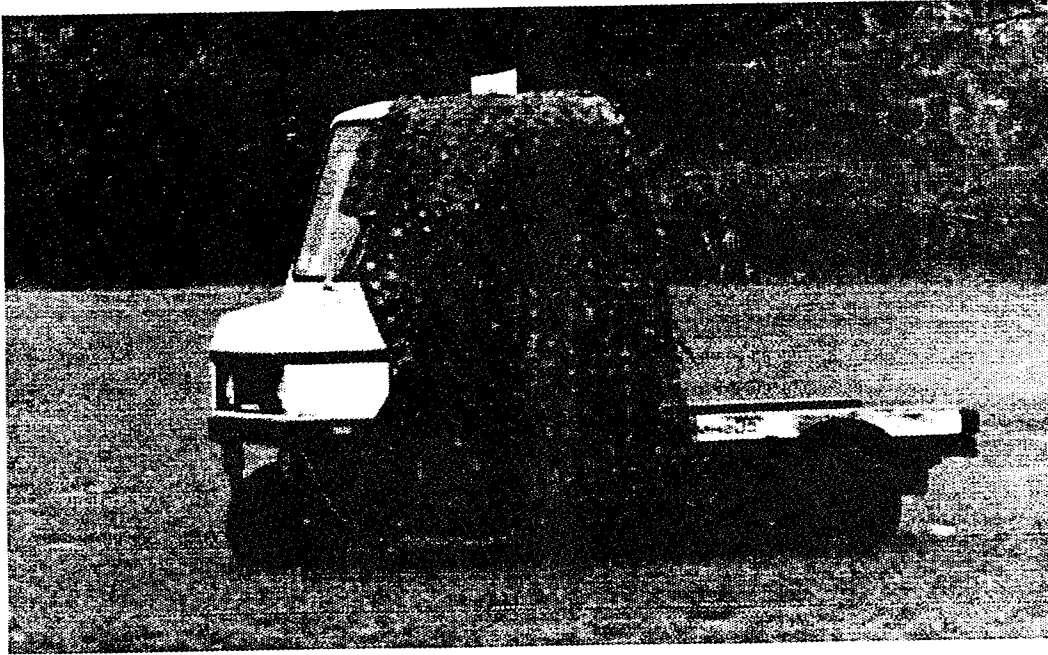

Figure 14. Car and camouflage #5.
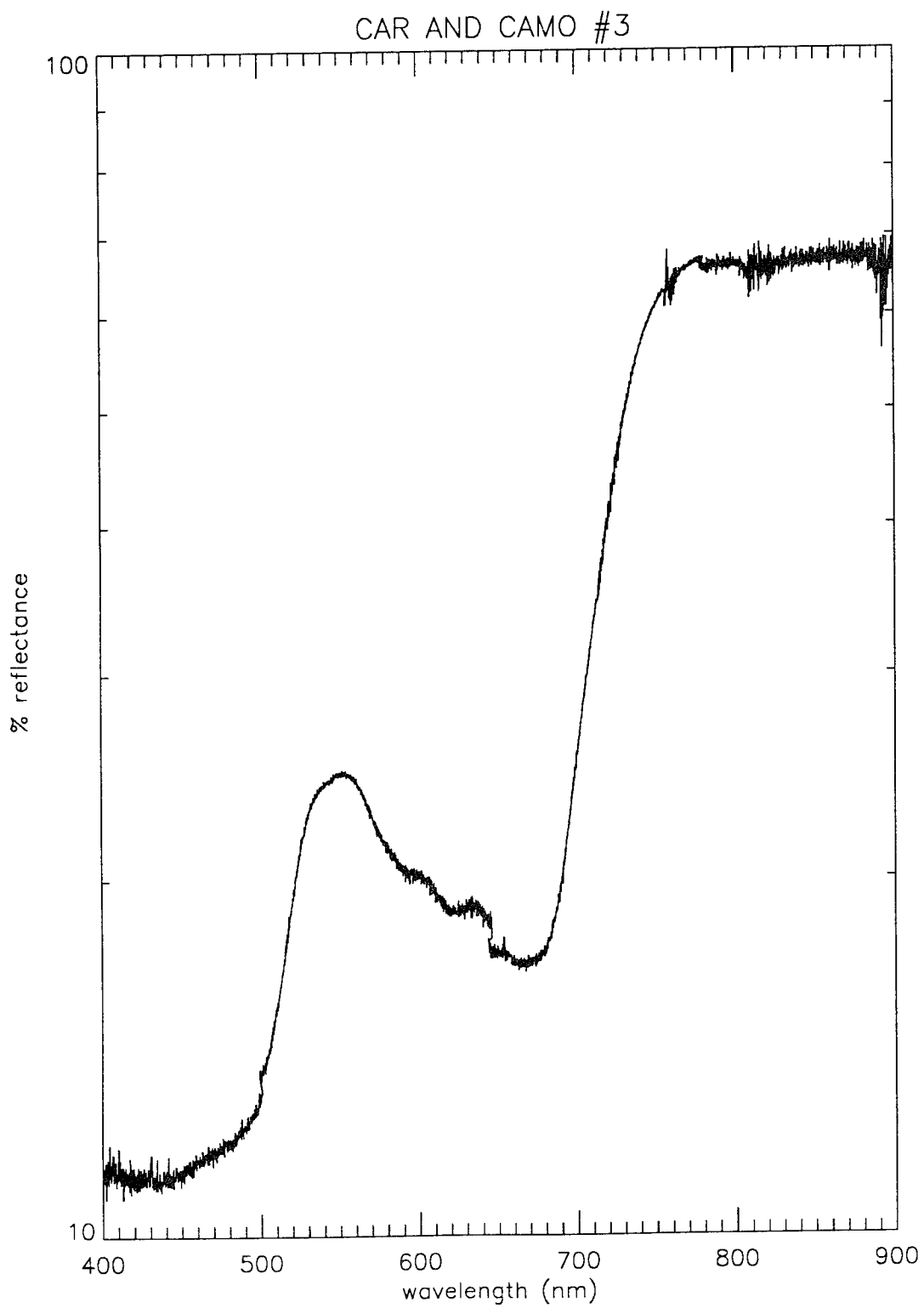
Figure 15. Cushman and camouflage #2

CAR AND CAMO #3

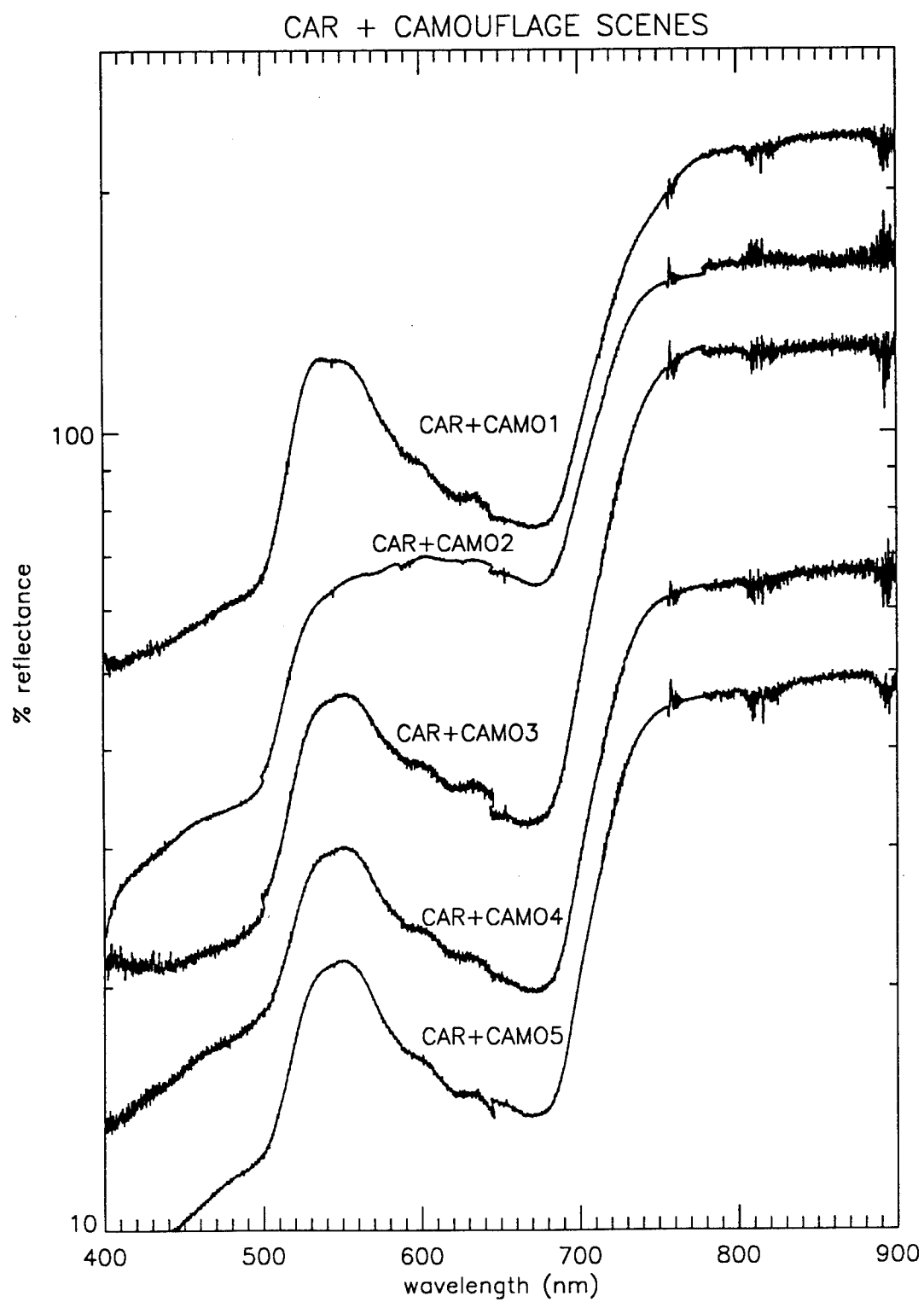Figure 16. Car and Camouflage #3.

Figure 17. Car and all camouflage scenes.

63

CUSHMAN + CAMOUFLAGE SCENES

CUSH+CAMO1

CUSH+CAMO2

CUSH+CAMO3

CUSH+CAMO4

CUSH+CAMO5

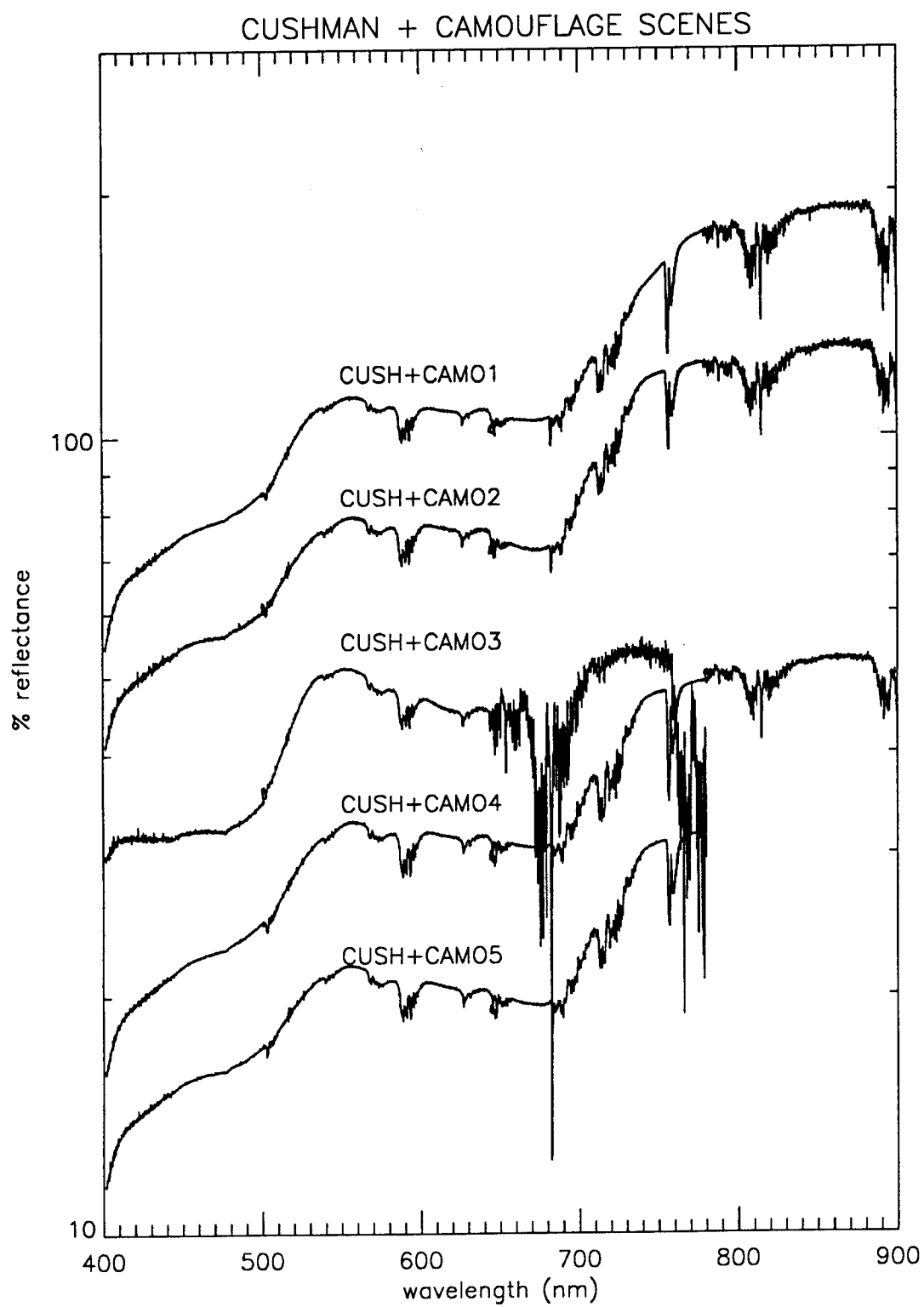% reflectance

100

10

wavelength (nm)

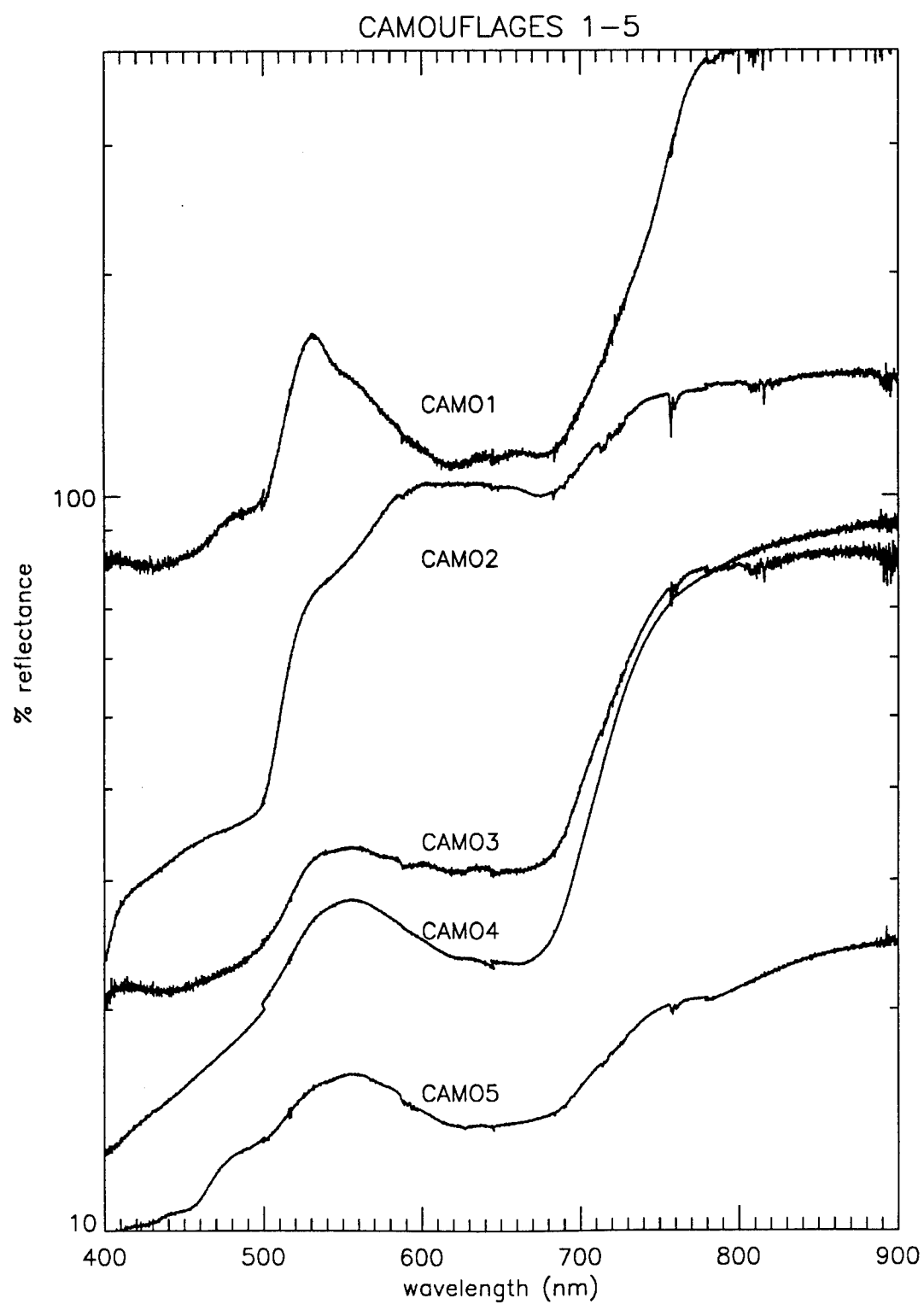Figure 18. Cushman and all camouflage scenes.

Figure 19. All camouflages.

65
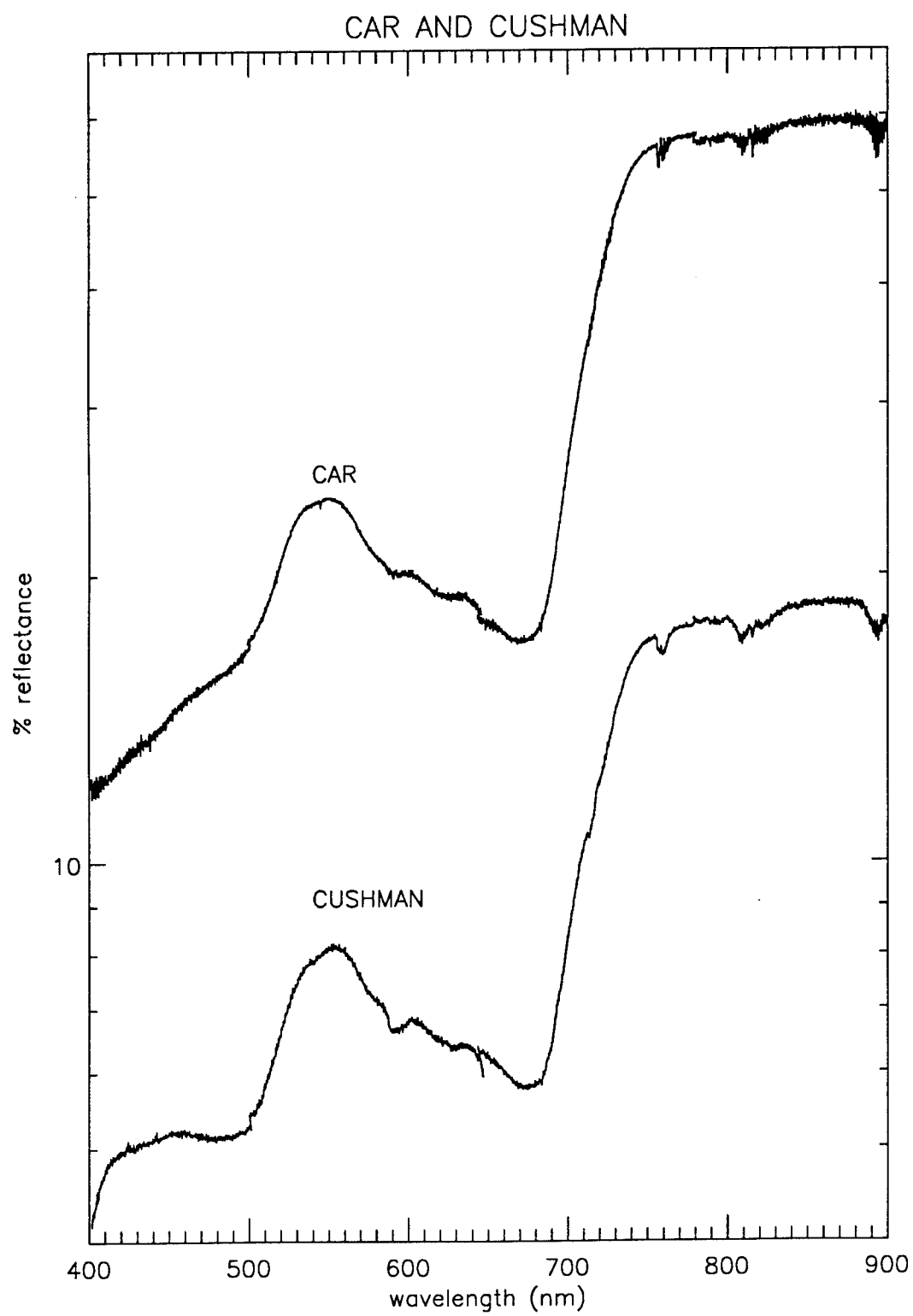
Figure 20. The car and cushman.
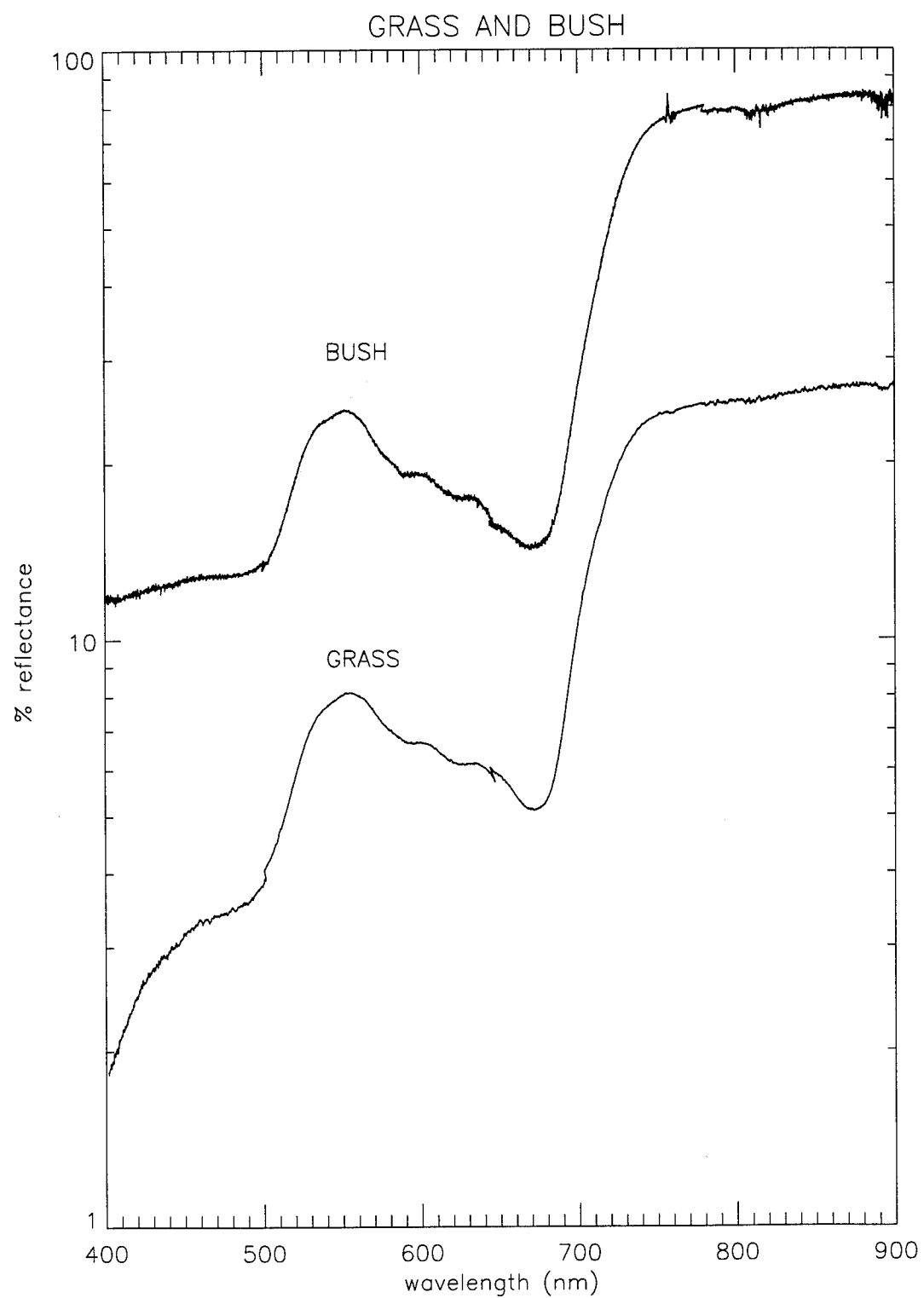
Figure 21. The grass and the bush.

CAR AND CAMO #3 TWO ENDMEMBERS

% reflectance

A=	0.990000
B=	0.0100000
C=	0.00000
D=	0.00000
RMS min	4.10000

wavelength (nm)
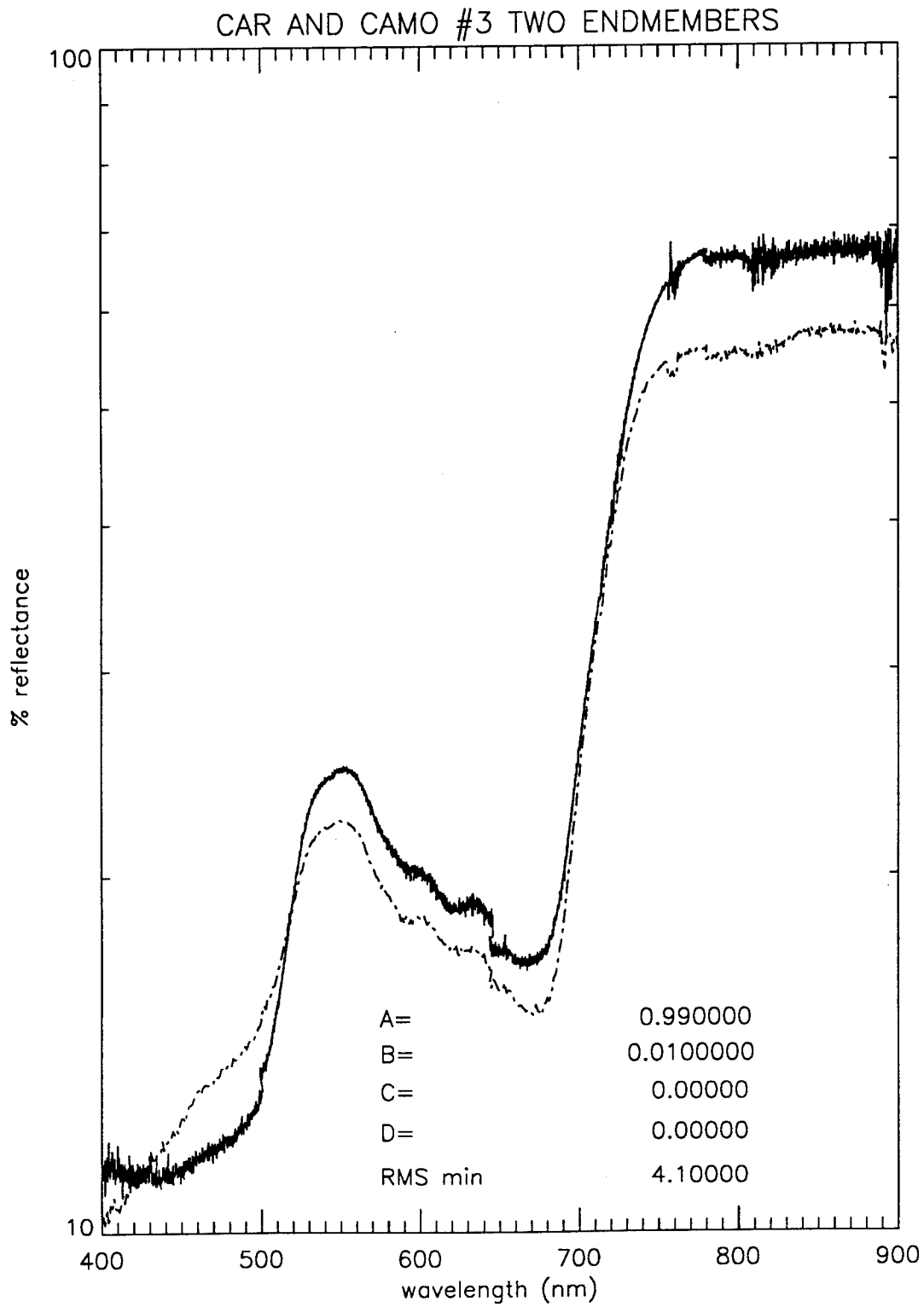
Figure 22. Car and camouflage #3 scene solid line, two endmember
best fit dotted line.

68

CAR AND CAMO #3 THREE ENDMEMBERS

A=	0.0600000
B=	0.490000
C=	0.450000
D=	0.00000
RMS min	1.12000
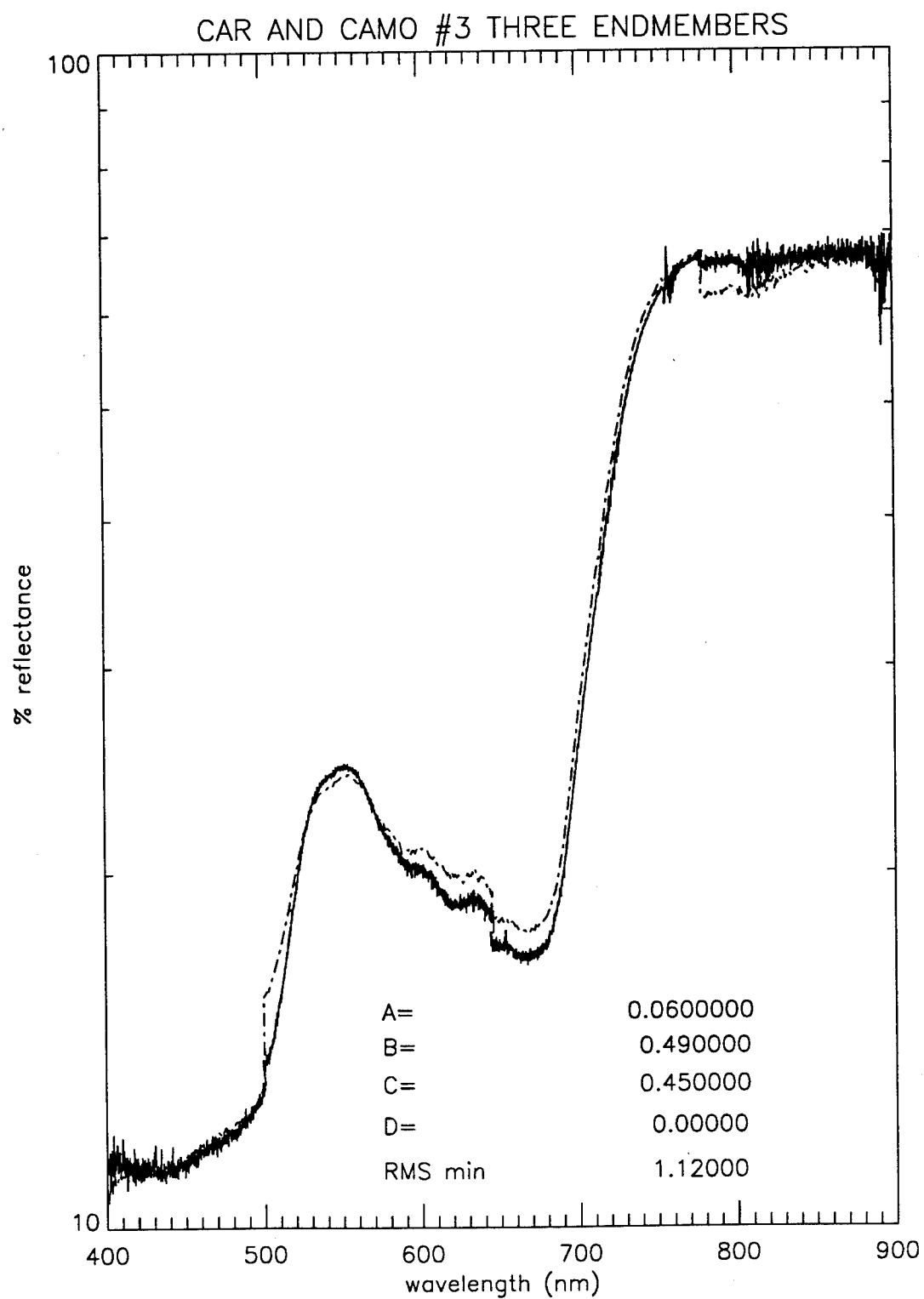
Figure 23. Car and camouflage #3 scene solid line, three endmember best fit dotted line.

69

CAR AND CAMO #3 FOUR ENDMEMBERS

A=	0.00000
B=	0.400000
C=	0.450000
D=	0.150000
RMS min	1.11000
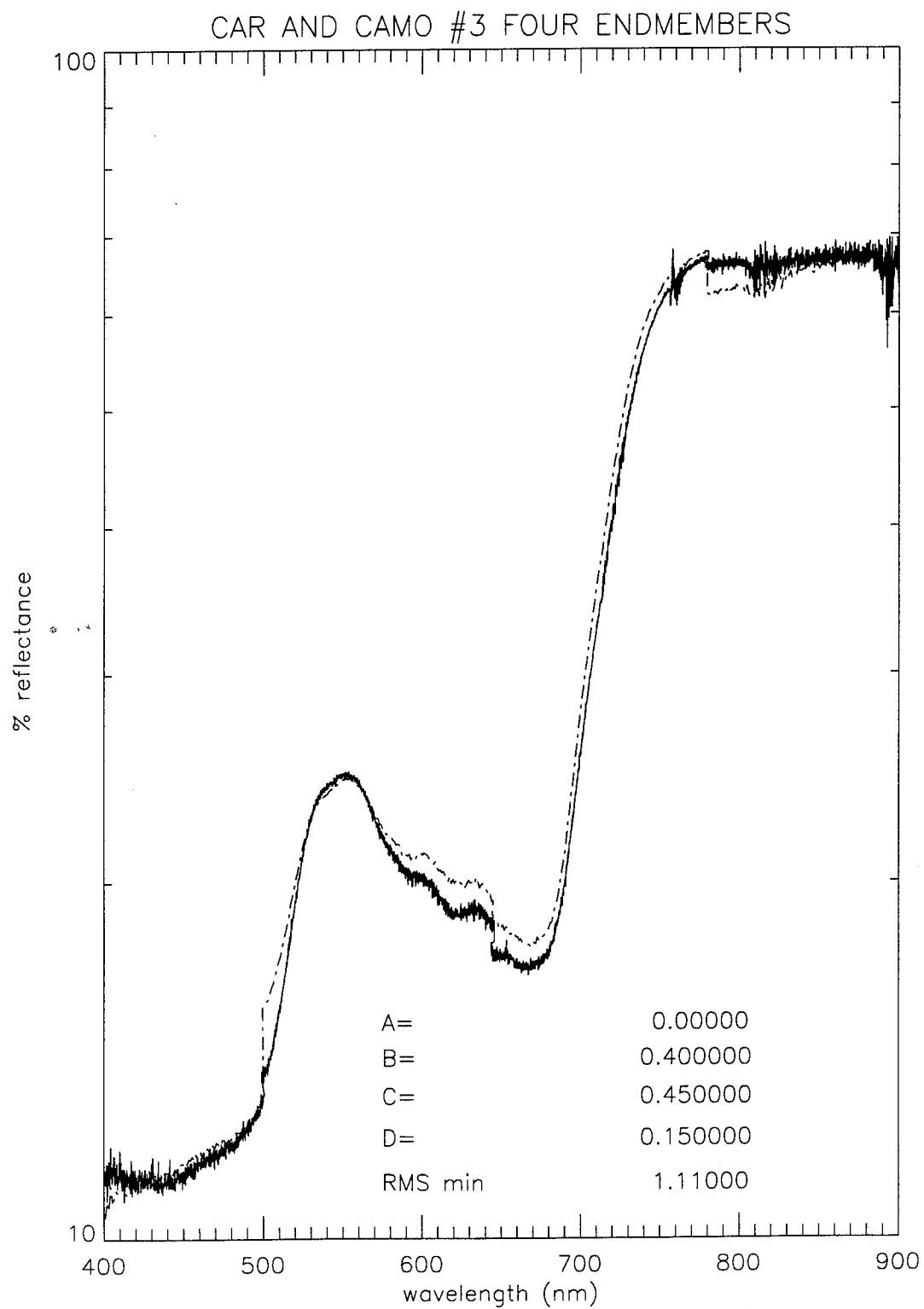
Figure 24. Car and camouflage #3 scene solid line, four endmember best fit dotted line.

CAR AND CAMO #4 ALLOWING NEG ENDMEMBERS

% reflectance

wavelength (nm)

A= 0.970000
B= -0.270000
C= 0.00000
D= 0.300000
RMS min 1.23000
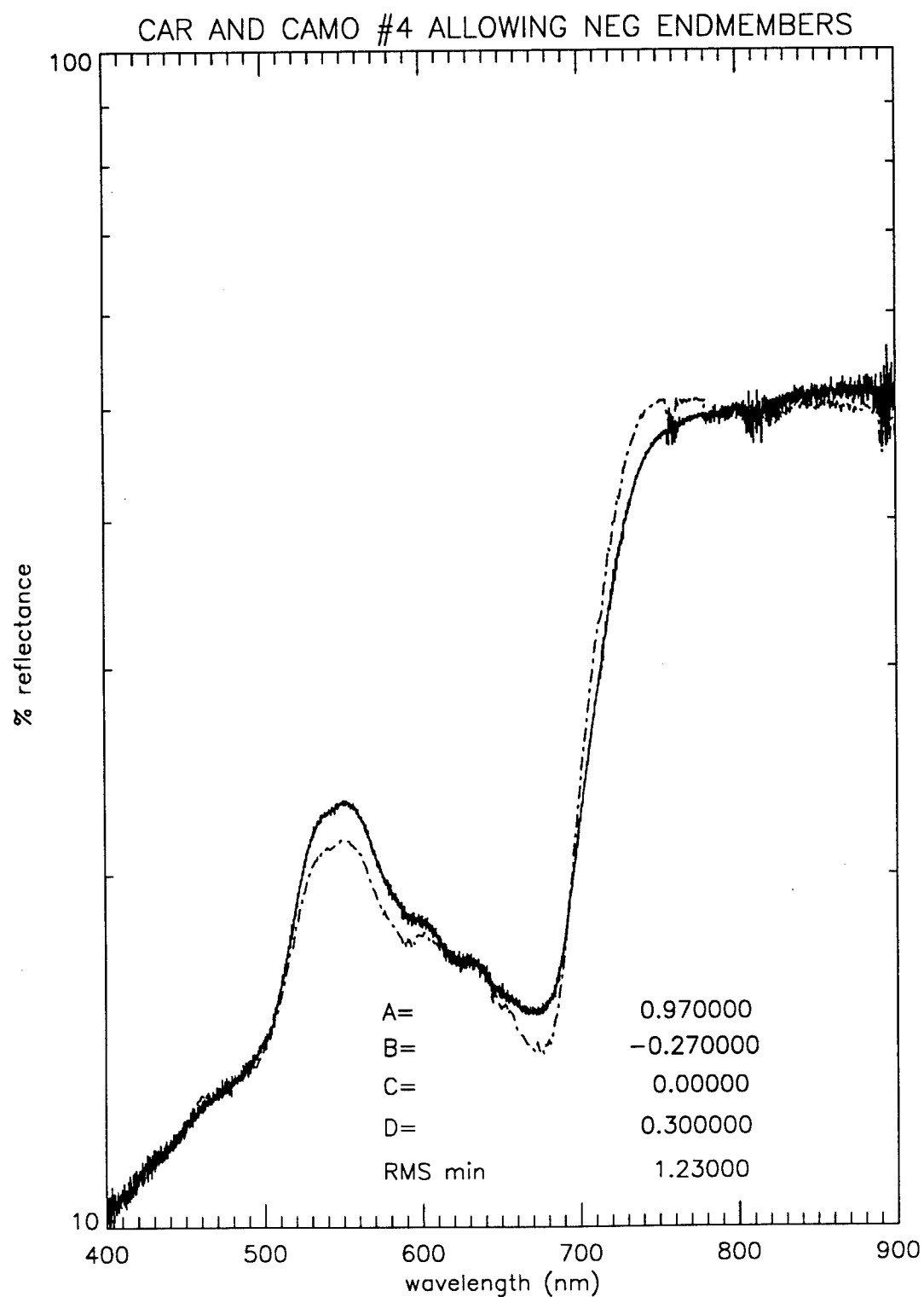
Figure 25. Car and camouflage #4 solid line, four endmember best
fit allowing negative endmembers dotted line.

71

CAR AND CAMO #3 FILTERED

	filtered	unfiltered
A=	0.0100000	0.00000
B=	0.690000	0.700000
C=	0.300000	0.300000
D=	0.00000	0.00000
RMS	4.31102	5.05392
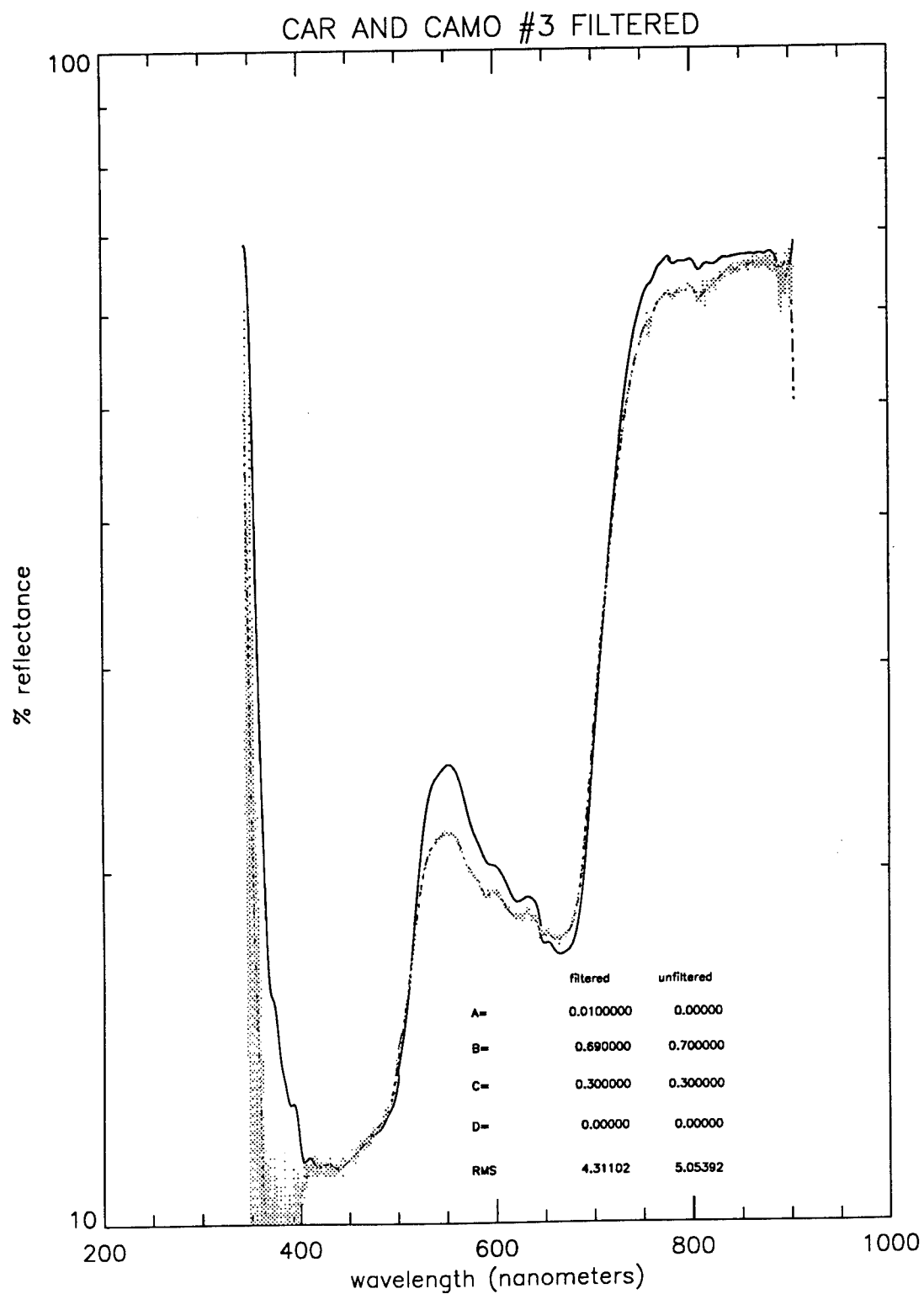
Figure 26. Car and camouflage #3: Both scene and best fit filtered. The scene is plotted as the solid line.

CAR AND CAMO #3 FILTERED

	filtered	unfiltered
A=	0.0100000	0.00000
B=	0.690000	0.700000
C=	0.300000	0.300000
D=	0.00000	0.00000
RMS	4.31102	5.05392

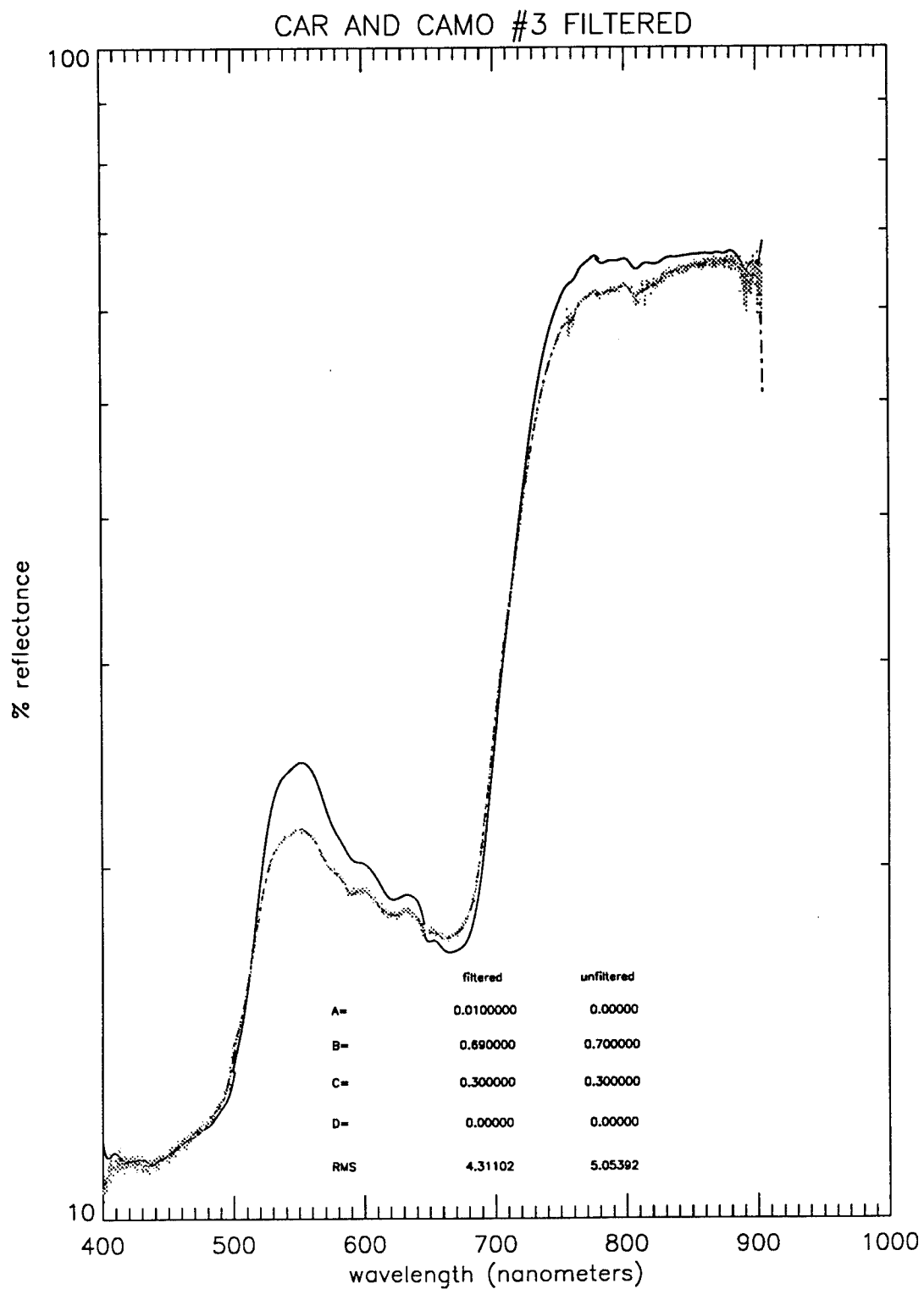Figure 27. Car and camouflage #3: Both scene and best fit filtered. The scene is plotted as the solid line.

APPENDIX B. MAYAN RUIN AND SHIP DATA

A. MAYAN RUINS

Kestrel Corporation took spectral data of the Mayan ruins and surrounding forest in Cavakmul Mexico to demonstrate the ability to locate a particular species of tree with a multi-spectral instrument. For reasons that are not completely understood, the Ramon tree only grows near Mayan ruins. If these trees can be located using spectral data, then Mayan ruins could be more easily located. These data sets are good examples of what may be typical spectra taken from an aircraft. The field of view of all the data sets contain forest background. At the ranges that the data was taken it is impossible to have a pure endmember. Given that no reliable endmembers are available, no attempt at linear spectral mixing and unmixing was made with this data. This could be an interesting test range for these techniques to determine if the structures could be detected under the canopy of the forest. By taking up close pure spectral measurements of the Ramon tree and the ruins, it may be possible to unmix these endmembers and accomplish the stated goal of finding Mayan ruins.

In the absence of a spectral mixing analysis, correlation coefficients were calculated between all the available data files. Table 8 lists the correlation coefficients for this data set. The available data sets and the abbreviations used in the table are as follows:

- Ramon #2 (RAM #2)-a tree taken from above.
- Ramon #1 (RAM #1)-same tree taken from the side with tree trunks visible.
- Acropolis under canopy (ACROP)-ruin structure hidden beneath forest canopy.
- Structure #7 (STRUC #7)-stone ruins partially visible in heavy forest.
- Guaya #1 (GUAYA)-near leafless tree in heavy forest surroundings.
- Distant mixed forest (FOREST)-heavy forest scene.

	RAM #2	RAM #1	ACROP	STRUC #7	GUAYA	FOREST
RAM #2	1.0000	0.9631	0.9372	0.9883	0.9519	0.9602
RAM #1	0.9631	1.0000	0.9479	0.9489	0.9653	0.9607
ACROP	0.9372	0.9479	1.0000	0.9366	0.9718	0.9952
STRUC #7	0.9883	0.9489	0.9366	1.0000	0.9422	0.9576
GUAYA	0.9519	0.9653	0.9718	0.9422	1.0000	0.9753
FOREST	0.9602	0.9607	0.9952	0.9577	0.9753	1.0000

Table 8. Correlation coefficients for Mayan Ruin data set.

It is interesting to see how well correlated the ruin structures (ACROP and STRUC #7) are to the forest and other vegetative spectra. In general these structures have a slightly lower correlation than the trees do to the other spectra. The two unexpected results are that the Acropolis under canopy is .9952 correlated to the forest and Structure #7 is .9883 correlated to Ramon #2. Figure 28 shows the spectra for these data sets plotted with a variable offset for presentation purposes. This shows that the spectra for the Acropolis under canopy and the mixed forest are indeed almost identical. Photographs of the region show scenes that are essentially identical. Not enough information is available to determine if the distant forest scene inadvertently contains a ruin structure in it or if possible the forest canopy is too thick to detect the structure. Contrast this with the spectra of Ramon #2 and Structure #7. Here there are differences in the spectra. The infrared ledge of the Ramon #2 is steeper and longer than that of the Structure #7.

B. SHIP DATA

Data was taken from the beach of two shrimp boats approximately 300 meters from the shore. Boats A and Boats B represent the same scene, but Boats B was taken 15

minutes after Boats A. Figure 29 shows the spectra of these three data sets. Table 9 gives the correlation coefficients for these data sets.

	OCEAN	BOAT A	BOAT B
OCEAN	1.0000	0.7442	0.8871
BOAT A	0..7442	1.0000	0.6816
BOAT B	0.8871	0.6816	1.0000

Table 9. Correlation coefficients for ship data.

This data is presented to introduce the possibilities of detecting a boat or ship on the ocean using spectral data. All three plots are noisy and similar in shape, but the boat scenes are clearly distinct from the open ocean scenes. The probable reason for Boat A and Boat B not being more highly correlated is an inconsistent field of view for the recording instrument. At 300 meters, the majority of the field of view is ocean and thus both Boat A and Boat B have a relatively high correlation coefficient with the ocean. Further analysis of this data is difficult without more information.
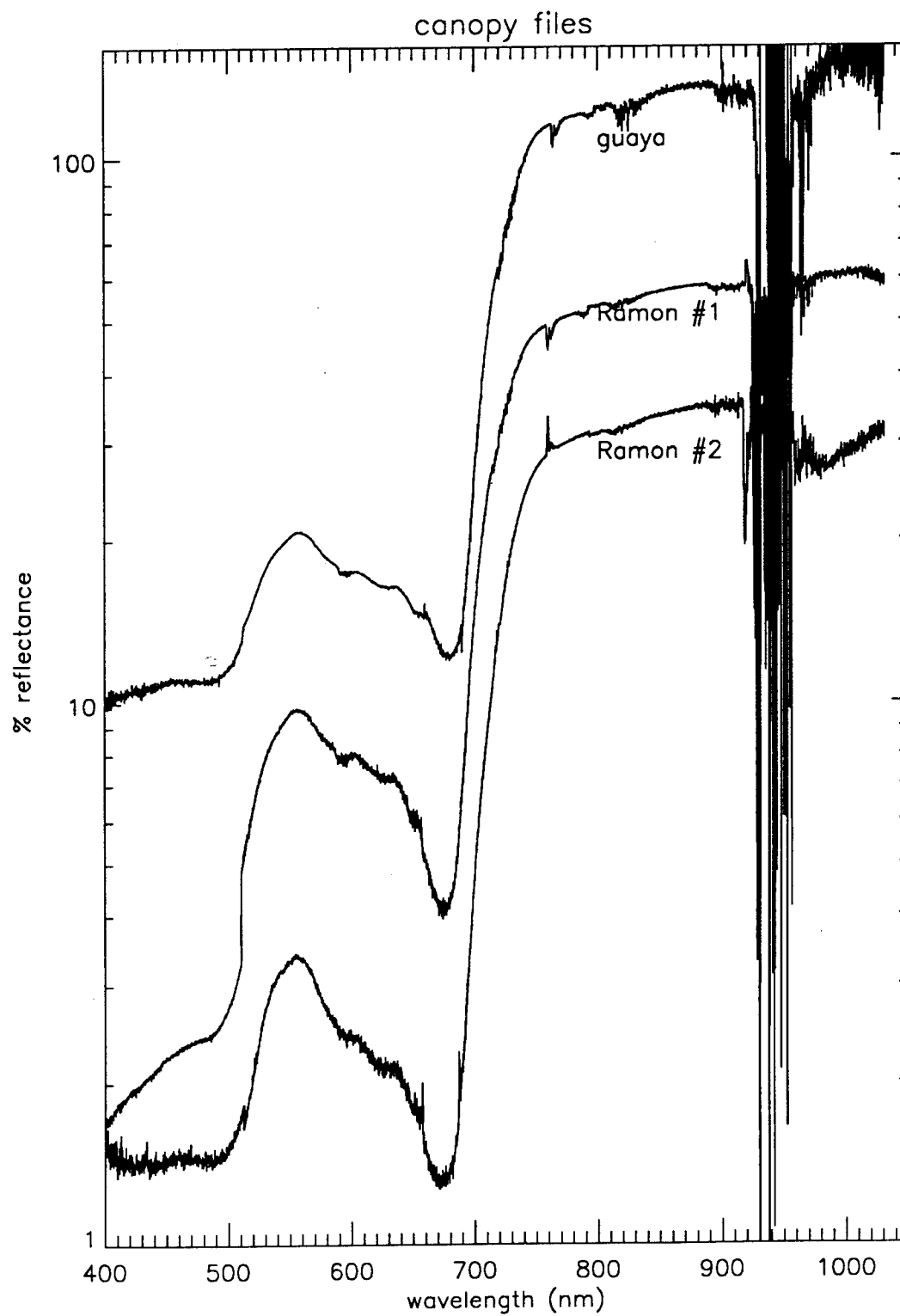
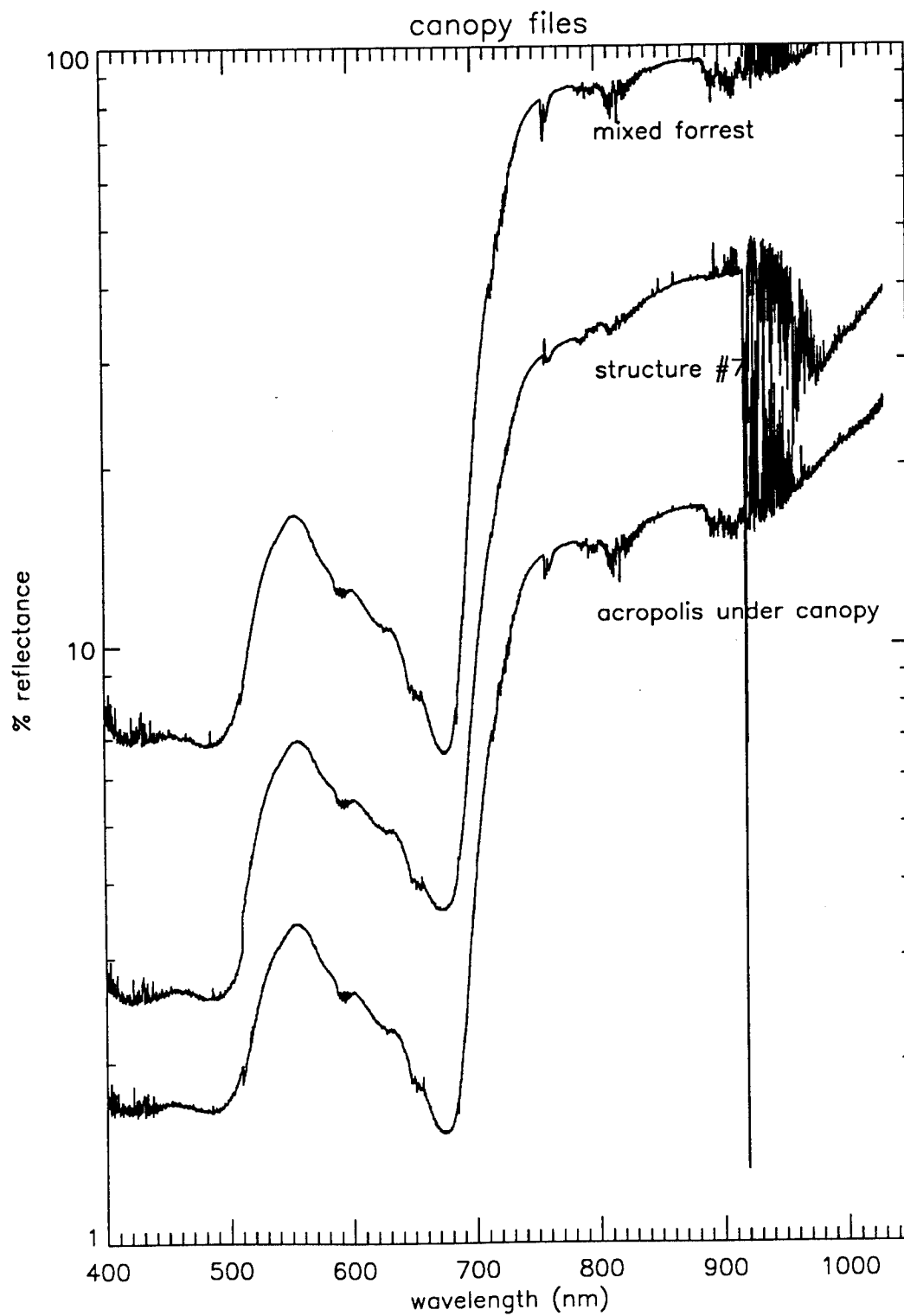canopy files

Figure 28 A. Mayan Ruin Files: Guaya tree and Ramon trees.

Figure 28 B. Mayan Ruin Files: Sturcture #7, Mixed forrest, and Acropolis.
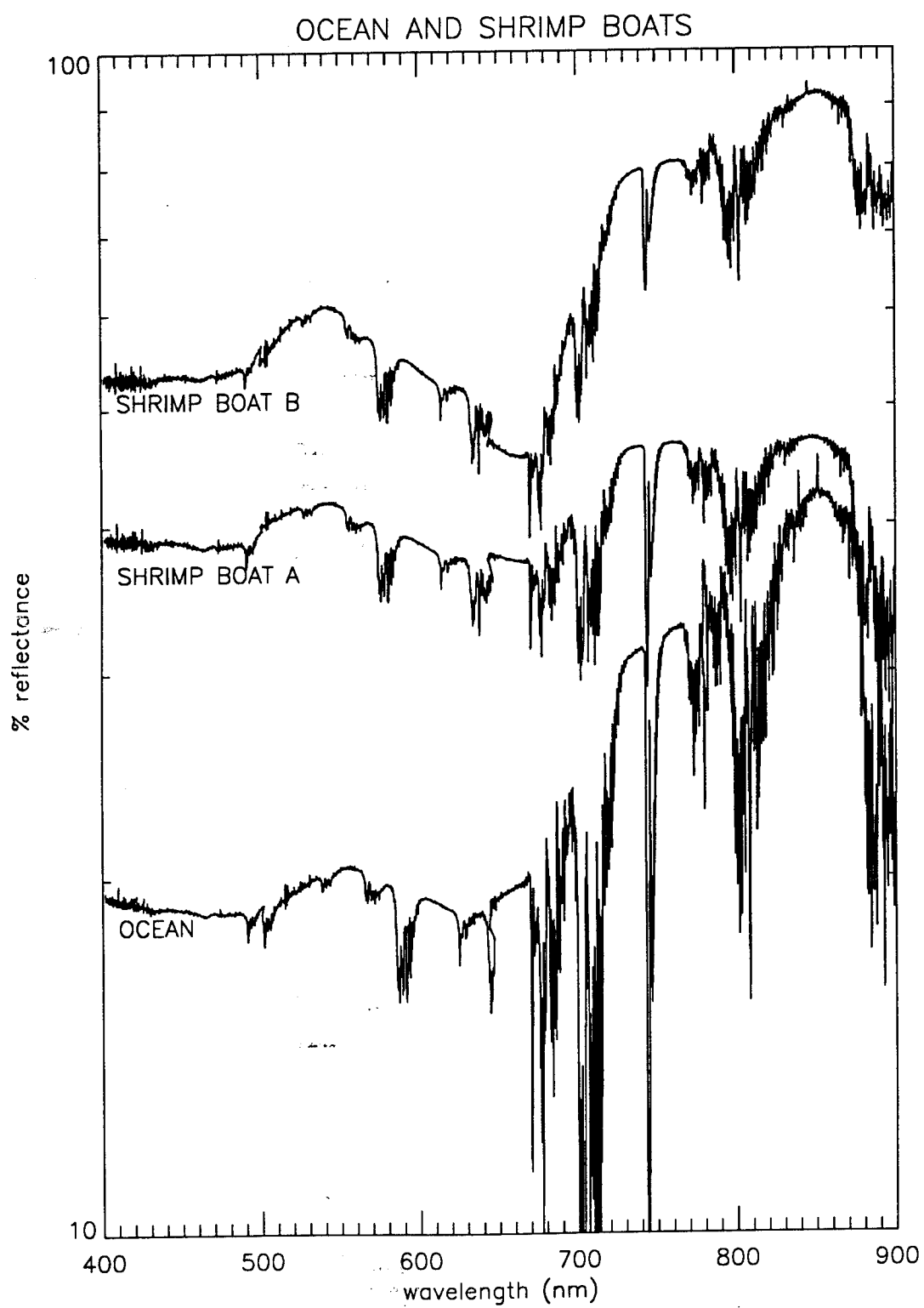
OCEAN AND SHRIMP BOATS

Figure 29. Ocean and shrimp boats.

80

LIST OF REFERENCES

Aboukhaled, A., 1966, Optical Properties of Leaves in Relation to their Energy-Balance, Photosynthesis, and Water Use Efficiency; Ph.D. Thesis, University of California Library, Davis, 139 p.

Adams, J.B., Smith, M.O., and Johnson, P.E., 1986, "Spectral Mixture Modeling: A New Analysis of Rock and Soil Types at the Viking Lander 1 Site," *Journal of Geophysical Research,* 91:8098-8112.

Allen, W.A., Gausman, H.W., and Richardson, A.J., 1969, "Interaction of Isotropic Light with a Compact Plant Leaf," *Journal of the Optical Society of America,* 59:1376-1379.

Allen, W.A., Gausman, H.W., and Richardson, A.J., 1970, "Mean Effective Optical Constants of Cotton Leaves," *Journal of the Optical Society of America,* 60:542-547.

Allen, W.A., and Richardson, A.J., 1968, "Interaction of Light with a Plant Canopy," *Journal of the Optical Society of America,* vol. 58 number 8, 1023-1028.

Barrett, E.C., and Curtis, L.F., 1976, Introduction to Environmental Remote Sensing (Second Edition), Chapman and Hall, New York, p. 258.

Boardman, J.W., 1990, "Inversion of High Spectral Resolution Data," Proceedings, SPIE, vol.1298: 222-233.

Breece, H.T. III, and Holmes, R.A., 1971, "Bi-Directional Scattering Characters of Healthy Soybeans and Corn Leaves," *Applied Optics,* 10:119.

Bunnik, N.J.J., and Verhoef, W., 1974, "The Spectral Directional Reflectance of Agricultural Crops," *NIWARS Publication 23.*

Bush, V. (Director), 1942, "Visibility Studies and Some Applications in the Field of Camouflage," Summary Technical report of division 16, NDRC, vol. 2: p. 3.

Condit, H.R., 1970, "The Spectral Reflectance of American Soils," *Photogrammetric Engineering and Remote Sensing,,* 36:955-956.

Dengler, N.G., 1982, "Leaf Anatomy," *Encyclopedia of Science and Technology,* vol.7 pp. 602-608, New York, McGraw Hill.

Department of the Army, 1968, Field Manual 5-20, Washington DC.

Gates, D.M., Keegan, H.J., Schleter, J.C., Weidner, V.R., 1965, "Spectral Properties of Plants," *Applied Optics,* 4:11-20.

Gausman, H.W., and Allen, W.A., 1973, "Optical Parameters of Leaves of 30 Plant Species," *Plant Physiol,* 52:57-62.

Gausman, H.W., 1977, "Reflectance of Leaf Components," *Remote Sensing of the Environment,* 6:1-9.

Gausman, H.W., Allen, W.A., Myers, V.I., and Cardenas, R., 1969, Reflectance and Internal Structure of Cotton Leaves, *Agronomy Journal,* 61:374-376.

Janza, R.J., 1975, in Manual of Remote Sensing, vol. 1 (Reeves et al., Eds), American Society of Photogrammetry, Falls Church, VA, p. 98.

Johannsen, C.J., 1969, The Detection of Available Soil Moisture by Remote Sensing Techniques; Ph.D. Thesis, Purdue University, p. 266.

Knipling, E.B., 1969, Leaf Reflectance and Image Formation on Color Infrared Film, Remote Sensing in Ecology, P.L. Johnson, Ed., University of Georgia Press, Athens, GA, pp.17-29.

Knipling, E.B., 1970, Physical and Physiological Basis for the Reflectance of Visible and Near-Infrared Radiation from Vegetation, *Remote Sensing of Environment,* 1:155-159.

Kubelka, P., and Munk, F., 1931, Ein Beitrag zur Optik der Farbanstriche, Zeitschr. Techn. Physik. 11:593-601.

Lillesaeter, G., 1982, Spectral Reflectance of Partly Transmitting Leaves: Laboratory Measurements and Mathematical Modeling, *Remote Sensing of the Environment,* 12:247-254.

Mendelsohn, John, Editor, 1989, Covert Warfare: Cover and Deception by the Royal Air Force in World War Two, Garland Publishing Inc., New York, NY.

Myers, V.L., Wiegand, M.D., and Thomas, J.R., 1966, Remote Sensing in Soil and Water Conservation Research, Proceedings Fourth Symposium on Remote Sensing of Environment, Institute of Science and Technology, University of Michigan, Ann Arbor, pp. 801-813.

Myers, V.I., 1983, in Manual of Remote Sensing, vol. II (Estes et al., Eds), American Society of Photogrammetry, Falls Church, VA, pp. 2136-2148.

National Defense Research Committee, 1946, Summary Technical Report of Division 16, Visibility Studies and Some Applications in the Field of Camouflage, Office of Scientific Research and Development, Washington, DC.

Oriel Corporation, 1994, Product Catalog, Stratford, CT.

Rao, V.R., Brach, E.J., and Mack, A.R., 1979, Bi-directional Reflectance of Crops and the Soil Contribution, *Remote Sensing of Environment*, 8:115-125.

Reit, S., 1978, Masquerade: The Amazing Camouflage Deceptions of World War II, First Signet Printing, New York, NY.

Saleh, B.E.A., and Teich, M.C., Fundamentals of Photonics, John Wiley and Sons, New York, NY, pp. 3-18.

Schuster, A., 1905, *Journal of Astrophysics,* 21, 1.

Sinclair, T.R., 1968, Pathway of Solar Radiation Through Leaves, M.S. Thesis, Purdue University, Lafeyette, IN.

Steiner, D., and Gutermann, T., 1966, Russian Data on Spectral Reflectance of Vegetation, Soil, and Rock Types, Final Technical Report, United States Army European Research Office.

Stokes, G.G., 1862, On the Intensity of the Light Reflected from or Transmitted Through a Pile of Plates, *Proceedings of the Royal Society,* 11:545-556.

Suits, G.H., 1972, The Calculation of the Directional Reflectance of a Vegetative Canopy, *Remote Sensing of Environment*, 2:117-125.

Thomas, J.R., Myers, V.I., Heilman, M.D., and Wiegand, C.L., 1966, Factors Affecting Light Reflectance of Cotton; Proceedings Fourth Symposium on Remote Sensing of Environment, Institute of Science and Technology, University of Michigan, Ann Arbor, pp. 305-312.

Thomas, J.R. Namken, L.N., Oerther, G.F., and Brown, R.G., 1971, Estimating Leaf Water Content by Reflectance Measurements. *Agronomy Journal* 63:845-847.

Tucker, C.J., 1980, Remote Sensing of Leaf Water Content in the Near Infrared, *Remote Sensing of Environment*, 10:23-32.

Whiffen, D.H., 1966, Spectroscopy, John Wiley and Sons, New York, NY.

Willstätter, R., and Stoll, A., 1918, Untersuchungen über die Assimilation der Kohlensäure, Springer, Berlin.

Woolley, J.T., 1971, Reflectance and Transmittance of Light by Leaves, *Plant Physiol*, 47:656-662.

INITIAL DISTRIBUTION LIST

1. Defense Technical Information Center
   Cameron Station
   Alexandria, Virginia 22304-6145 2

2. Library, Code 52
   Naval Postgraduate School
   Monterey, California 93943-5101 2

3. William B. Colson, Code PH/Cw
   Naval Postgraduate School
   Monterey, California 93943-5002 1

4. Richard C. Olsen, Code PH/Os
   Naval Postgraduate School
   Monterey, Californai 93943-5002 2

5. Radian Inc. attn: Larry W. Cartier
   Suite 725, Huntwood Plaza
   5845 Richmond Highway
   Alexandria, Virginia 22303-1865 1

6. Kestrel Corp. attn: John Otten
   6020 Academy Blvd NE
   Suite 104
   Albuquerque, New Mexico 87109 2

7. Dr J. Rafert
   Department of Physics and Space Sciences
   150 West University Blvd
   Florida Institute of Technology
   Melborne, Florida 32901 1

8. Anthony T. Chandler
   P O Box 2541
   University of Arkansas at Monticello
   Monticello, Arkansas 71656-2541 1

9. Lt John W. Chandler
   126 Westwood Lane
   Monticello, Arkansas 71655 1

10. Lt Suzanne E. Lyon
    1050 Kensington Dr
    Roseville, California 95661 1